NBSIR 77-1270

Materials For Fuel Cells

L. H. Bennett, M. I. Cohen, A. L. Dragoo, A. D. Franklin,
A. J. McAlister and K. F. Young

Institute for Materials Research
National Bureau of Standards
Washington, D.C. 20234

Annual Report - January 1976 to December 1976

Issued May 1977

Prepared for

Division of Conservation Research and Technology
U.S. Energy Research and Development Administration
Washington, D.C. 20545

NBSIR 77-1270

MATERIALS FOR FUEL CELLS

L. H. Bennett, M. I. Cohen, A. L. Dragoo, A. D. Franklin,
A. J. McAlister and K. F. Young

Institute for Materials Research
National Bureau of Standards
Washington, D.C. 20234

Annual Report - January 1976 to December 1976

Issued May 1977

Prepared for
Division of Conservation Research and Technology
U.S. Energy Research and Development Administration
Washington, D.C. 20545

U.S. DEPARTMENT OF COMMERCE, Juanita M. Kreps, *Secretary*

Dr. Sidney Harman, *Under Secretary*

Jordan J. Baruch, *Assistant Secretary for Science and Technology*

NATIONAL BUREAU OF STANDARDS, Ernest Ambler, *Acting Director*

1. Introduction

The National Bureau of Standards has undertaken a program of research on materials for fuel cells. This program includes studies of electrocatalysis in liquid-electrolyte cells and of the solid electrolyte in high-temperature cells. The overall objectives of the program are:

1. to provide data allowing selection of optimum materials for critical aspects of fuel cell operations;
2. to improve the measurement capability and standards for assessment of performance (e.g., efficiency of electrode processes and lifetime of components) of materials in fuel cells.

This report will describe the results for the first year of the program.

The Materials for Fuel Cells Program at NBS consists of three major elements, which taken together reinforce each other in techniques and concepts; these elements embrace:

i. electrocatalysis, especially oxygen reduction, on non-metallic surfaces;

ii. electrocatalysis, especially hydrogen oxidation, on non-noble metals and alloys; and

iii. degradation mechanisms involving solid oxygen-transporting electrolytes. Items ii and iii received ERDA funding during the past year and are the subject of this report.

2. Subtask Reports

2.1 Non-Noble-Metal Electrocatalysts

2.1.1 Electrocatalysis on Non-Noble Metals and Alloys

Introduction

A limiting factor in full scale implementation of the low temperature acid fuel cell for electric power production is the scarcity and expense of Pt, the current material of choice for fuel and oxygen electrocatalysts. In the search for adequate non-precious substitutes for Pt, the "refractory hard metals" - alloys of transition metals with carbon, boron, nitrogen, etc. - offer a promising area of investigation, for they are transition-metal-like: they have d-band vacancies, have refractory properties, and display considerable chemical stability. A number of these materials have in fact been found to be active for the oxidation of hydrogen in acid electrolyte. A survey is presented in Table 1.

Table 1 lists the corrosion potential, where available, in volts relative to the standard hydrogen potential, with the compound. Most of these studies have been carried out in H_2SO_4. Activity in H_3PO_4 has been observed for WC and $(Mo_{0.8}W_{0.2})C$, the latter for the first time in our laboratory, in the course of the present work. A number of these compounds have no practical use in fuel cells, either because of low corrosion potentials, or because their activity is very low. The latter are indicated in Table 1 by the notation 1.a.

Our overall task under this contract is the search for non-precious substitutes for Pt as fuel electrocatalysts, and proceeds along three general lines: 1) preparation and characterization of materials; 2) screening of these materials for stability in hot phosphoric acid; and

Table 1. Materials for which H_2 oxidation activity has been observed in acid electrolyte.

	IV	V	VI	VII	VIII		
3d				MnP_3(0.02)(l.a.)	FeP(0.08) FeP_2(0.30) FePS	CoP(0.05) CoP_3(0.25) CoPS(0.30) CoAsS $CoAs_2$(0.20) $CoAs_3$(0.25)	NiP_2(0.30)(l.a.)
4d			$Mo_{0.8}W_{0.2}C$(0.6) MoS_2 (l.a.)				
5d			WC (0.6) WS_2 (l.a.)				

Numbers in parenthesis are oxidation potential in volts relative to the standard hydrogen potential. Low activity is devoted by (l.a.). Materials are classified according to column (Roman numerals) and row in the Periodic Table of the host transition metal.

Sources: the present work, in particular $Mo_{0.8}W_{0.2}C$;
H. Bohm and F. A. Pohl, Wiss. Ber. AEG-Telefunken, 41, 46 (1968); K. Mund, G. Richter, and F. v. Sturm, Coll. Czech. Chem. Com., 36, 439 (1971); K. Mund, G. Richter, R. Schulte, and F. v. Sturm, Ber. der Bunsen-Gesell, 77, 839 (1973); G. Luft, K. Mund, G. Richter, R. Schulte, and F. v. Sturm, Siemen Forsch. u. Entwickl. Ber., 3, 177 (1974).

3) examination of acid-stable materials for electrocatalytic activity through potentiodynamic and steady-state current-voltage measurements. A summary of our work in these areas for the past year follows.

Acid Stability Measurements

To date, 55 alloys have been tested for stability in hot (82 °C), concentrated (85%) phosphoric acid. These materials are listed in Table 2. Of the 55, 18, denoted by blocks in the table, have shown stability, in that no gas was evolved, and no change in color of solution or alloy occurred. Several other materials (not noted in the table) reacted only slowly, and they will be investigated electrochemically, since they may have small but useful electrical ranges of stability.

Voltammetric Studies

Thus far, the following materials have been examined by cyclic voltammetry, in 1M H_3PO_4 (22 °C): W_2C, W_2B_5, WC, Mo_2C, $(Mo_{0.8}W_{0.2})C$, MoB, TaN, TaB, TaC, Pt, W, Mo, and two stainless steels, PH 15-7 Mo and PH 17-7. Hydrogen oxidation was observed only on Pt, WC, and $(Mo_{0.8}W_{0.2})C$. The activity of WC was found to be a function of preparation method; results for three WC samples are given in Table 3. The compound $(Mo_{0.8}W_{0.2})C$, which has the WC structure, was shown, for the first time, in the course of this work, to catalyze the oxidation of hydrogen in acid electrolyte. Its performance is compared with that of our most active WC sample in Figure 1. Both samples were porous, flooded electrodes consisting of powdered material (-325 mesh) bonded by dilute addition of Teflon. At the level of activity of these carbides, these electrodes should operate near unit effectiveness factor [1]. The

Table 2. Stability of some metals, alloys and "refractory hard metals" in hot phosphoric acid.

	IV	V	VI	VII	VIII		
3d	TiC [TiN] TiB_2	VC VB VB_2	Cr_3C_2 Cr_7C_3 $Cr_{23}C_6$ CrB CrB_2		FeB Fe_2B FeP FeSe $Fe_{40}Ni_{40}P_{14}B_6$ Stainless: [PH 15-7Mo] [PH 17-7]	Co_2P	Ni_3P Ni_3M_gB Ni_2TiAl Ni_5La
4d	[ZrC] ZrN ZrB_2	NbC Nb_2C NbN NbB NbB_2	["MoC"] [Mo_2C] [MoB] [$(Mo_{.8}W_{.2})C$] [MoS_2] Mo				
5d	HfC HfN HfB_2	[TaC] Ta_2C [TaN] [TaB] [TaB_2] [Ta]	[WC] W_2C [WB] [W_2B] [W_2B_5] [WO_3] [WS_2] [W]	[Re]			[Pt]

Table 3. Dependence of H_2 electrocatalytic activity of WC on the method of carbide preparation.

SAMPLE NO.	FORM	PREPARATION	H_2 OXIDATION CURRENT PER UNIT CAPACITANCE AT +0.3 VOLTS (RHE)
1	foil	$W + CH_4$	2.1×10^{-3} A/F
2	powder	W + C	3.0×10^{-3} A/F
3	powder	WO_3 + C	17.1×10^{-3} A/F

Preparation and Support:

1) Sheet, formed by exposing W sheet, 13μm thick, to a 5% CH_4-95% H_2 mixture for 4 hours at 1500 °C. Supported on epoxy.

2) Commercially obtained powder, formed by direct reaction of W with carbon. Supported on Ta sheet.

3) Powder, formed by heating WO_3 and carbon powder for 2 hours at 1800 °C in H_2. Supported on Ta sheet, and on Au with Teflon bonding.

Current is normalized to capacitance, evaluated from the sweep rate and current at +0.3 volts with respect to a relative hydrogen electrode (RHE).

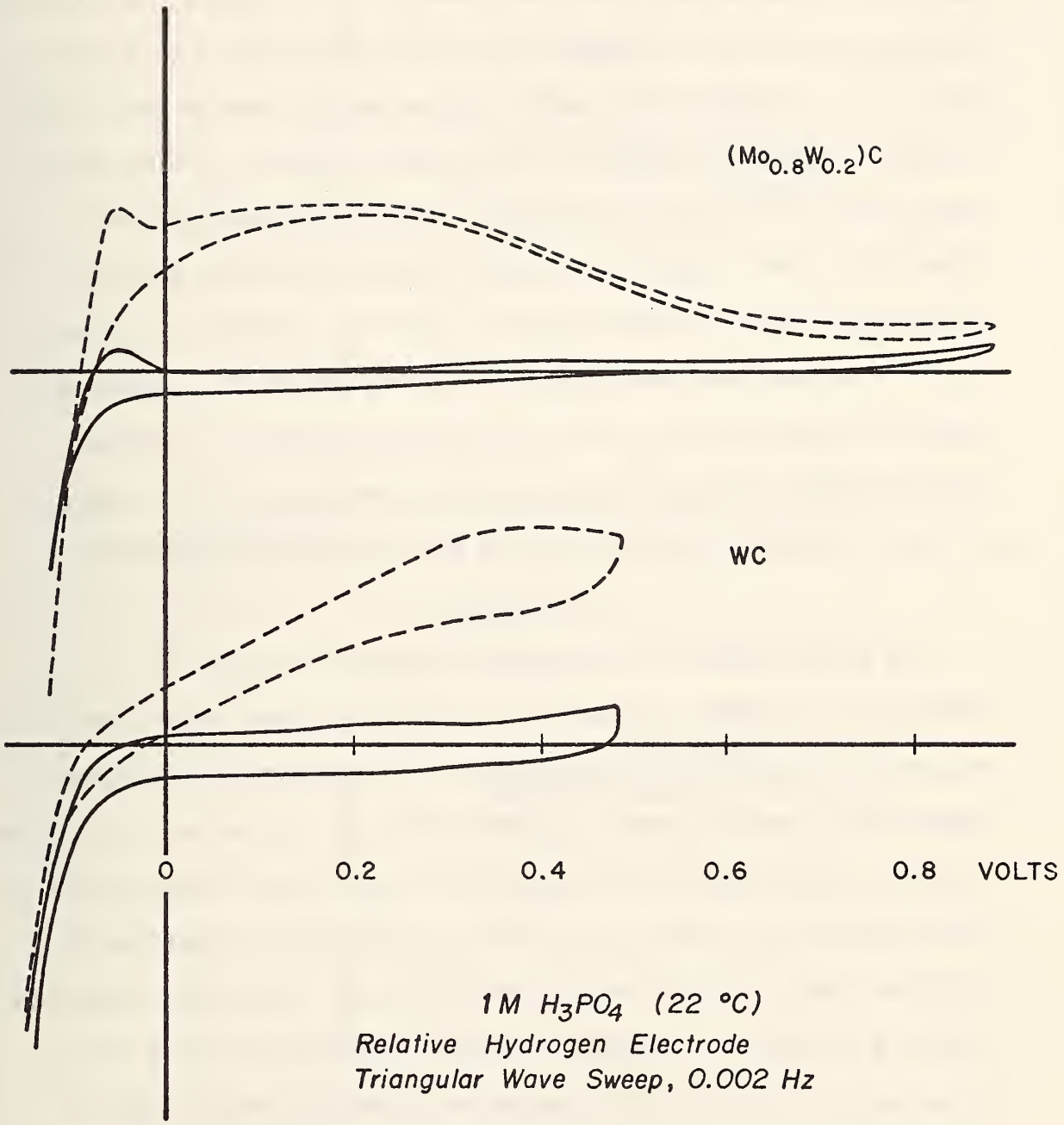

Figure 1. Cyclic voltammetric curves (RHE) for $(Mo_{0.8}W_{0.2})C$ and WC: H_2 oxidation in 1 molar (M) phosphoric acid (22 °C)

current scales in Fig. 1 are identical but the current amplitudes do not directly reflect relative activity. The $(Mo_{0.8}W_{0.2})C$ electrode was smaller in gross surface area, and thinner. On this basis, we estimate $(Mo_{0.8}W_{0.2})C$ to have a maximum specific activity from 1.5 to 3 times greater than that of the WC sample, perhaps more, since we were forced to clean Fe grinding contaminant from the Mo carbide, a process which favors loss of fines from the powder. Several materials displayed potentially useful stability in acid, though no catalytic activity. Voltammetric data for three materials - Ta, TaN, and TaB - are shown in Fig. 2. The two stainless steels, PH 15-7 Mo and PH 17-7, showed wide ranges of stability, from -.4 to +3.2 volts (relative to a hydrogen electrode, RHE) but displayed noticeable capacitance in this range.

2.1.2 Microprocessor Controlled Electrochemical Measurements

Introduction

The proper design of an automated measurement system for laboratory use depends strongly on the parameters under investigation in the course of the controlled experiment. Decisions as to instrument capabilities, however, must allow flexibility or the end result might be a single purpose device whose usefulness is zero after completion of its initial objective. With this in mind, we examined the experimental technique used in electrochemical investigations and decided on what we feel is a satisfactory approach to automatic control and data taking. It is useful at this point to review the technique normally used so that basic criteria governing the design of the automated system will be evinced.

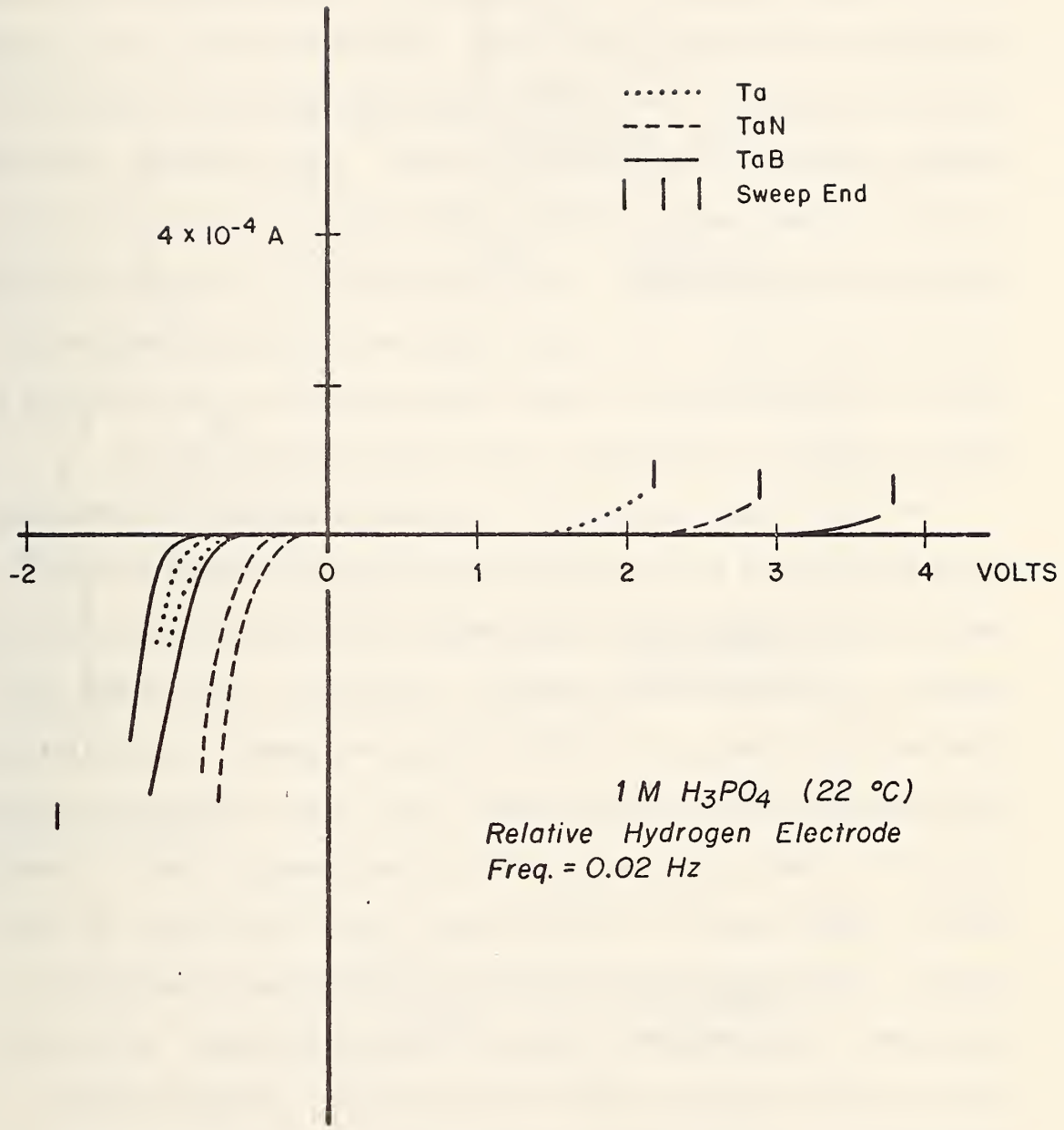

Figure 2. Cyclic voltammetric curves (RHE) for Ta, TaN and TaB showing absence of catalytic activity: 1 M phosphoric acid (22 °C) with bubbled nitrogen.

The potentiostat is the basic instrument used for this class of experiments. It consists (Fig. 3) of an error amplifier which measures the difference between an input potential and the potential drop between a reference electrode and the working (sample) electrode; this potential drop is a function of the current through the cell, i.e., from the counter electrode to the working electrode. The difference (amplified) is fed to a power amplifier which alters the cell current until the difference (error) is zero. The input potential to the potentiostat may be dc or ac voltages. The ac wave shape may be whatever the operator desires with the frequency range (typically dc-10 Hz) governed only by the characteristic impedances of the overall system [2].

The most common experimental arrangement consists of a motorized potentiometer used to generate an input potential (triangular wave-shape), which is fed to the potentiostat. With the addition of an X-Y recorder and the cell, the equipment is complete. Going beyond this experimental minimum, we can find varying arrangements of oscillators, stepping-motor-driven voltage sources, etc., used to generate the input potential. These allow the use of dc, linear sweeps (ramps), triangular sweeps, stepped sweeps, sine wave input, square wave input, and pulse inputs. Compensation for changes in potentials due to the IR drop across the cell's internal impedance is sometimes added. We may also find varying arrangements for output recording: two-pen recorders, logarithmic recorders, digital voltameters, etc [2]. With all this in mind, system design can proceed.

Basic Design Criteria

Experimentally, the system must be able to generate dc and ac potentials of variable wave shape. It must be capable of both analog

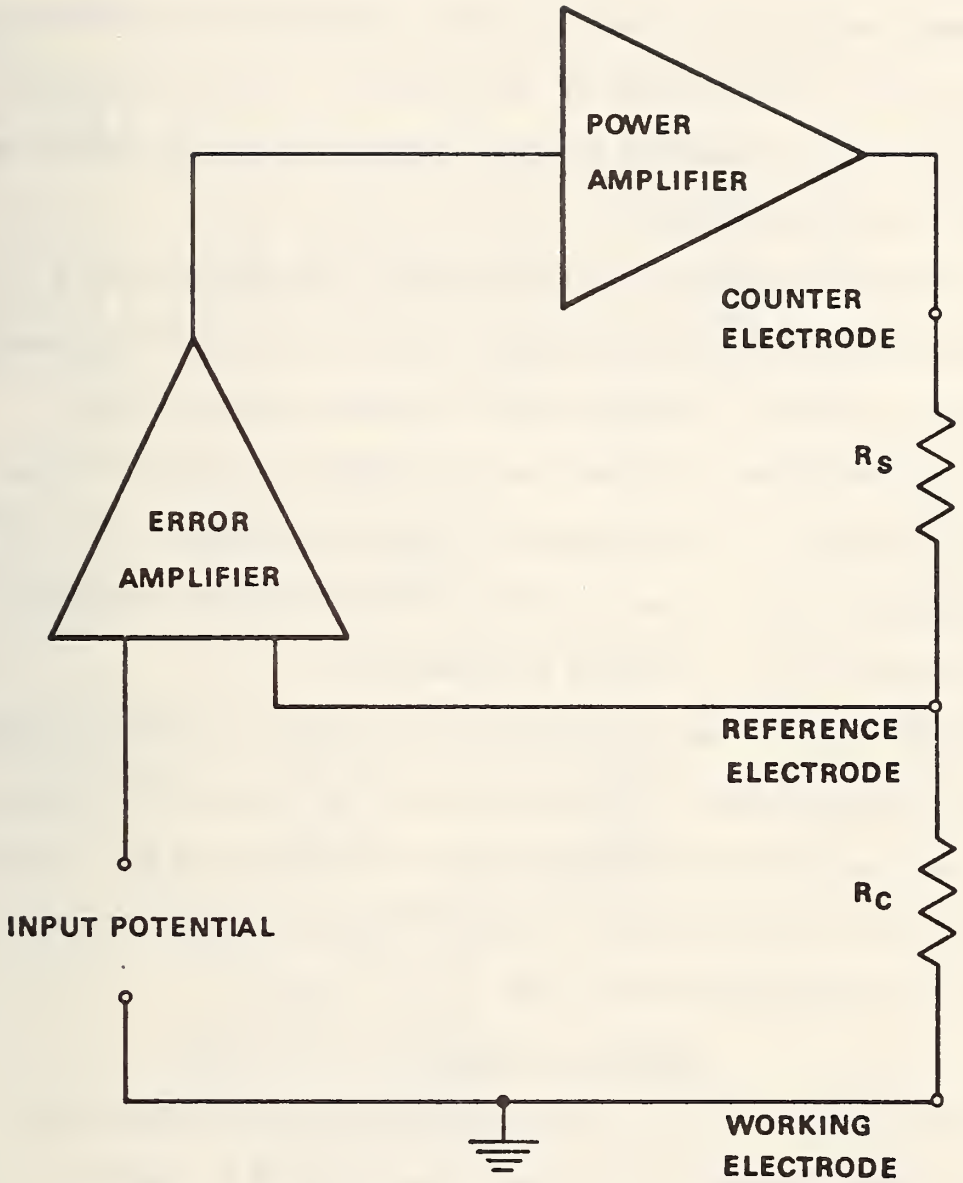

Figure 3. Simplified block diagram of a potentiostat. R_s is the effective series impedance produced by the counter electrode and the cell electrolyte R_c is the effective impedance (due to the flow of current through the cell) between the reference and working electrodes, which develops the measured potential.

and digital outputs of data. Control of the format of both input and output must be simple and fast. Once started, the apparatus must be able to operate unattended and must be able to terminate the experiment according to criteria established by the operator. It must be capable of communication with a computer for data analysis or else be capable of performing the analysis itself.

All of these functions can be performed by a system consisting of appropriate digital-to-analog and analog-to-digital converters combined with a digital computer. Although use of a central computer with a communication line to the experiment was considered, we decided to use a dedicated processor as a large computer would be under-utilized in the control functions of our system. Similar considerations of utilization also led to elimination of standard minicomputers.

The choice thus narrows to the usage of the desk calculator systems or of the new microprocessors. Cost considerations mandated the microprocessor approach which in retrospect appears to be a wise one. Since these devices are relatively new, a survey of their characteristics is desirable for understanding their usage in this system.

The Microprocessor

The microprocessor [3] is a single-chip large-scale integrated circuit (IC) which contains all the basic functions of a computer's central processing unit (Fig. 4). The differences between the two result mainly from in a difference in word size, with the microprocessor having a word of 16 bits or less. The smaller word size means a smaller instruction repertoire and smaller directly addressed memory capability. The most commonly available units at reasonable cost use an 8-bit word.

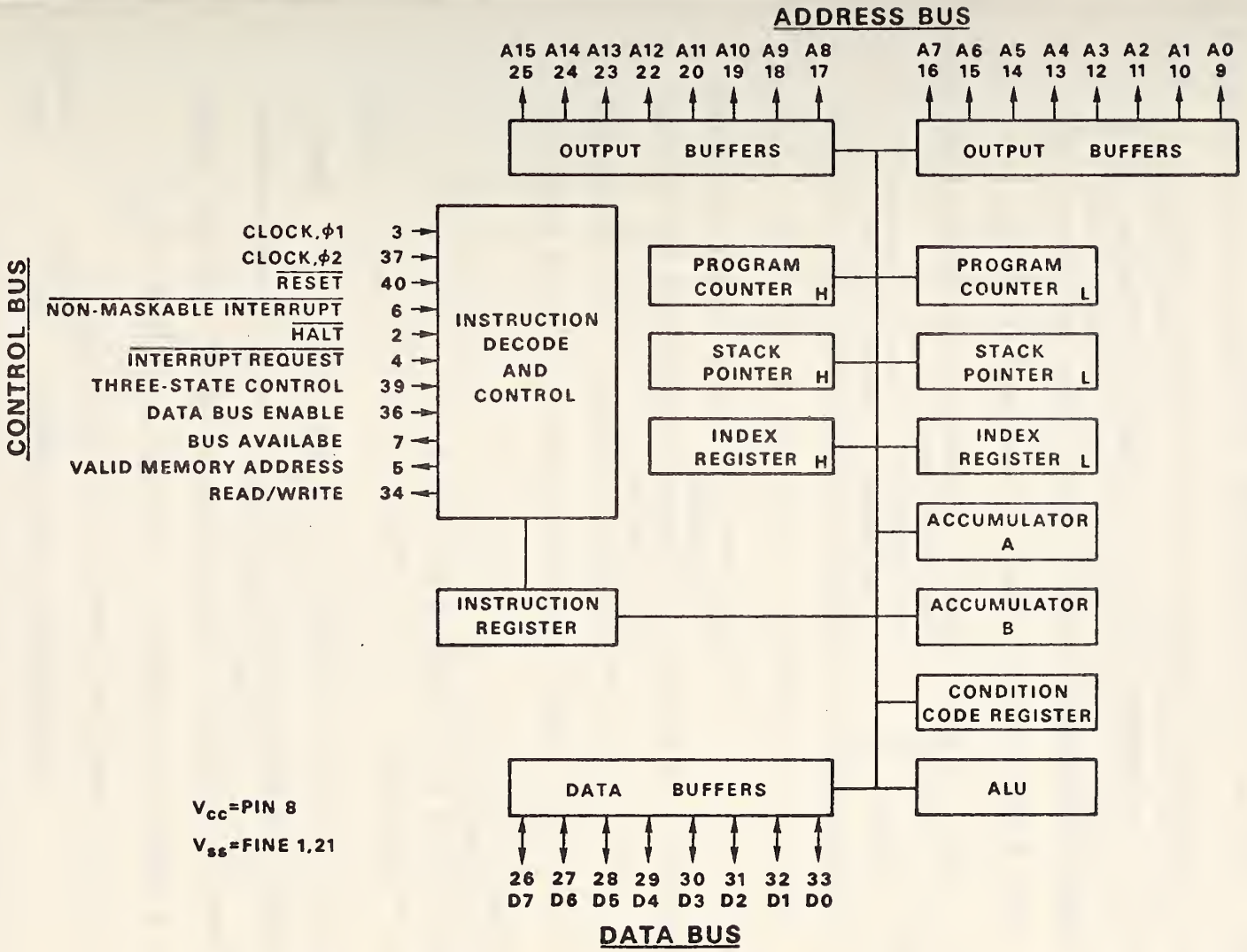

Figure 4. Block diagram of the internal organization of a typical microprocessor IC. H indicates the uppermost 8 bits of a 16-bit register. L is the lower 8 bits.

These 8-bit processors fall roughly into 2 classes. One class has both control and arithmetic functions of a relatively high order (e.g., 6800, 8080, Z-80, etc., processors), while the other class has restricted arithmetic functions and is better suited for control purposes only (F-8, SC/MP, etc.). Of the first class, the 6800 type is more readily utilized where input-output functions are of prime importance. As outlined under design criteria, there is some need for arithmetic capability. Thus, the 6800 type of microprocessor was selected for our application.

All of these units utilize what is known as bus-oriented architecture. That is, all signals of a common type are run via a common set of transmission lines to all devices requiring them. Each device has decoders so that it responds only to those signals meant for it. As indicated in Fig. 4 there are, in general, 3 buses: the address bus (unidirectional), the control bus (unidirectional) and the data bus (bidirectional).

When assembled with appropriate other devices: memory IC's, peripherals, logic IC's, clock, etc. (Fig. 5), a microcomputer results [4]. With the 6800 this arrangement has a capability of 2^{16} memory locations and a minimum instruction time of 2 μs. Data are received from peripherals by a memory read operation, and data are sent to peripherals by a memory write operation. Communication with a large computer or a very remote peripheral is via the modem.

Microcomputer Configuration

As noted above, we are using a 6800 microprocessor, with its associated support circuits (clock, gating circuits, etc.), as the basic element of our control system [5]. Along with this we have approximately

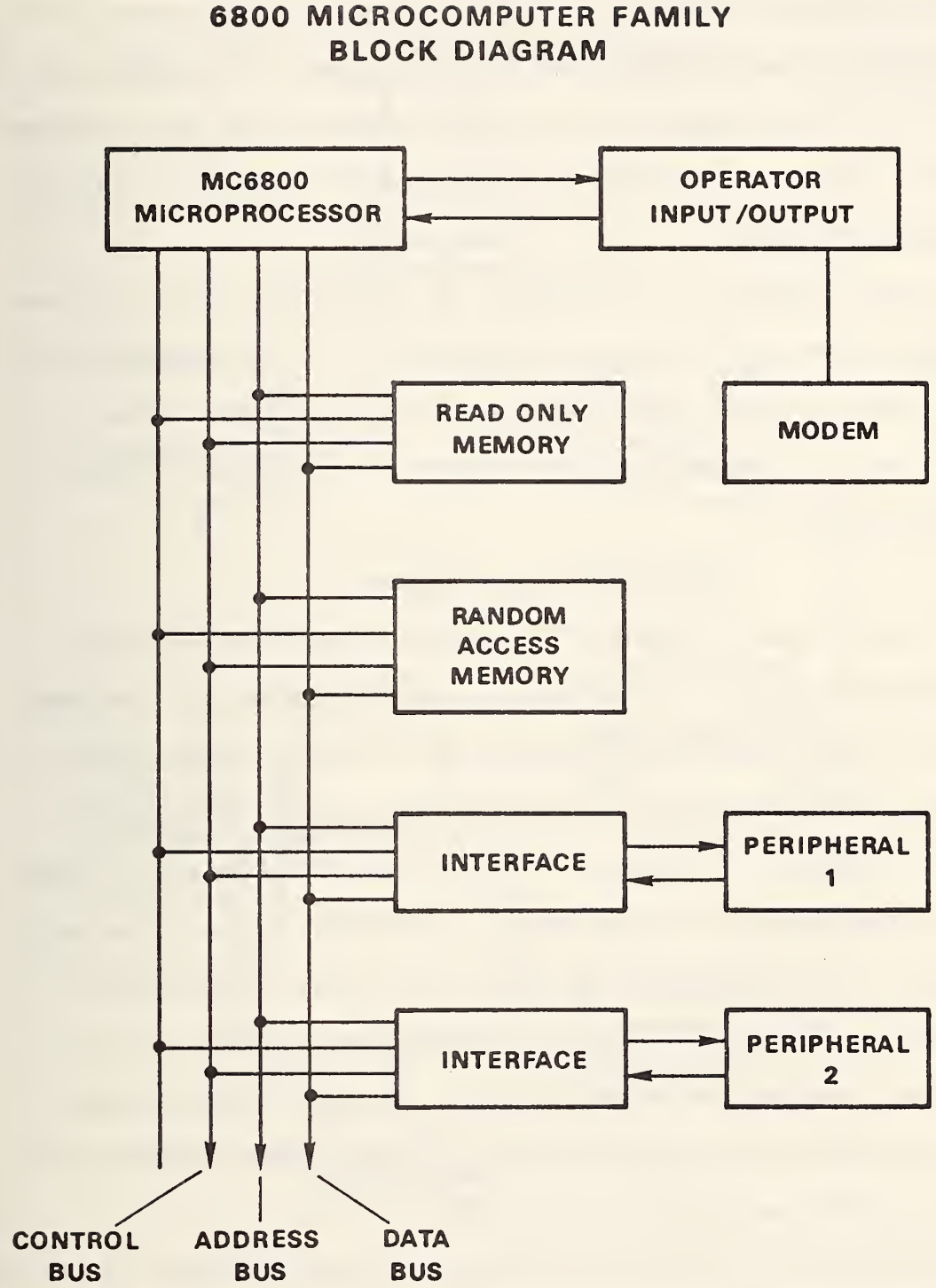

Figure 5. Block diagram of the typical organization of a microcomputer.

4,000 bytes (1 byte = one 8-bit word) of ROM (read only memory) storage. We also have about 12,000 bytes of RAM (random-access memory = read and write memory) storage. An interface is provided which allows communication with either the operator or an external computer. We use a teletype at present. Interface circuitry is also provided for use with a magnetic type cassette recorder.

Two other interfaces are provided. One communicates with a software programmable timer, while the other communicates with the conversion (or control) printed circuit board. The overall configuration is shown in Fig. 6. Each of the elements of the system will be discussed in detail in subsequent sections.

Main Printed Circuit Board

The central processing unit (CPU) and the input/output interfaces are contained on one (15 x 25 cm) board. The CPU consists of: the 6800 processor, a 1-MHz 2-phase clock, 1000 bytes of ROM, 640 bytes of RAM, and signal gating circuitry [6]. The three buses (data, address and control) are brought out through the 86-pin interconnection plug. There are three interfaces built on the board. One enables communication with the terminal at either 10 or 30 characters per second; communication with a central computer is, at present, through this terminal. The other two are reserved for future additions. One will handle a modem for direct communication with the central computer, while the other will provide high speed parallel data output [6].

An auxiliary (10 x 15 cm) board contains the power-on-reset circuit [6] and the cassette tape recorder interface. This board will be removed in the near future when a terminal with built-in cassette recorders arrives. An overall view of the input/output arrangement is shown in Fig. 7.

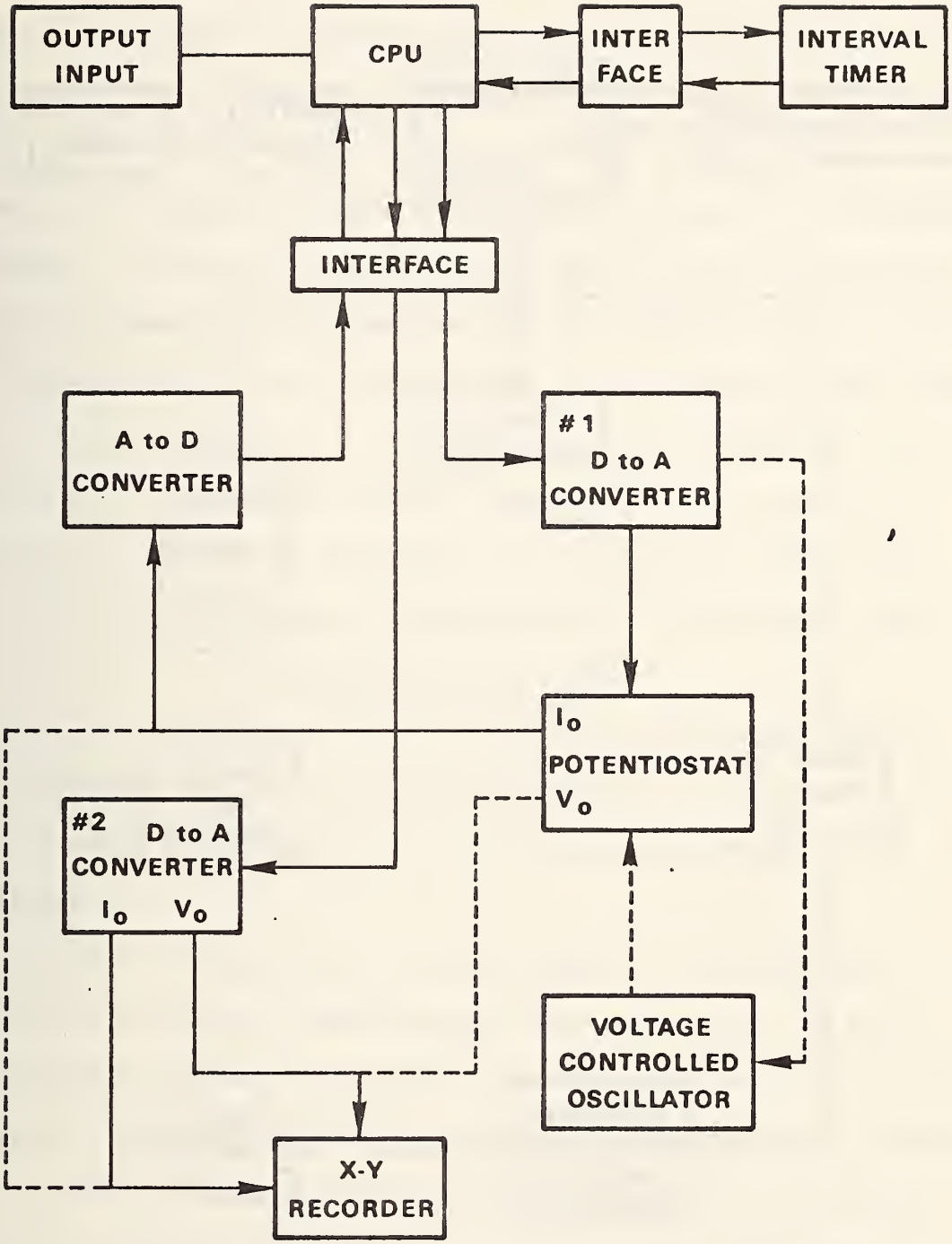

Figure 6. Black diagram of overall configuration of the microprocessor controlled electrochemical system.

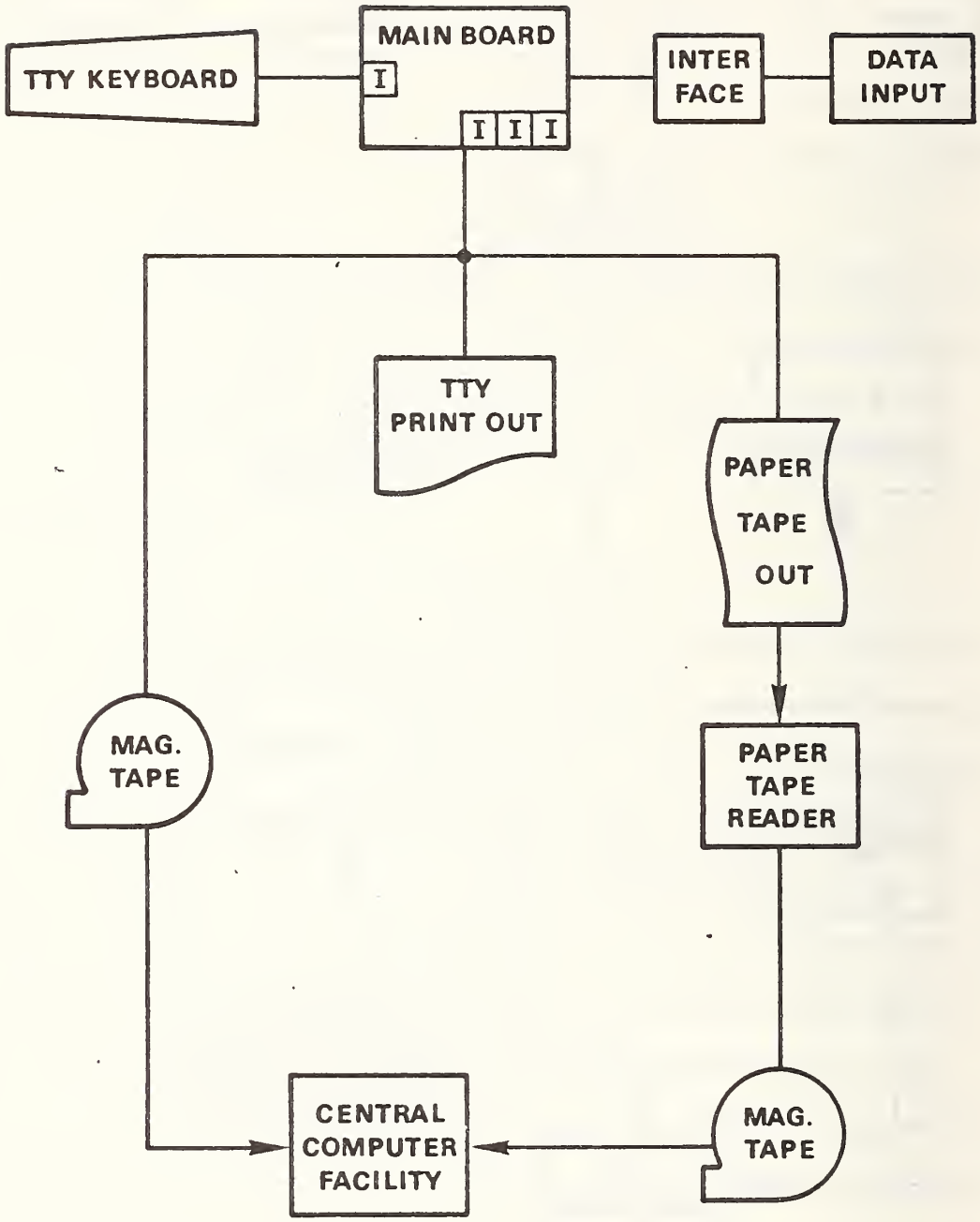

Figure 7. Input/output configuration of the system.

Memory Boards

There are three (15 x 25 cm) printed circuit boards, each containing 4,000 bytes of RAM. They are operable by simply inserting them into the 86-pin interconnection frame containing the buses, power, etc. At present, one is used for program storage which is loaded via the input/output arrangement. The others are used for data storage during the experiment.

A fourth memory board is designed and under construction. It will contain up to 8,000 bytes of reprogrammable ROM (at present we have 3000 bytes). There also will be an on-board programmable circuit so that a new program may be inserted when desired. Completion of this board will prevent loss of program on power failure (or turn-off) but will allow us the flexibility to change our operating system to accommodate needs.

Conversion (Control) Board

This (15 x 25 cm) board (Fig. 8) contains a programmable interval timer and interface, 2 digital-to-analog converters and interfaces, an analog-to-digital converter with its interface and a multiplexing circuit [7].

The interval timer [6] has a timing range of 1 μs to 42.6 min. The CPU sets the desired interval between points and starts the timer. When the period has elapsed, the timer signals the CPU which then reads the data via the analog-to-digital converter and checks to see if another point is needed. If so, the CPU stores, then outputs the data, resets the timer and repeats the process.

The two digital-to-analog converters (DAC) are identical 10-bit units. They have an output range of -5 to +5 volts and have a conversion time of about 1 μs. However, the CPU time to output a point is such

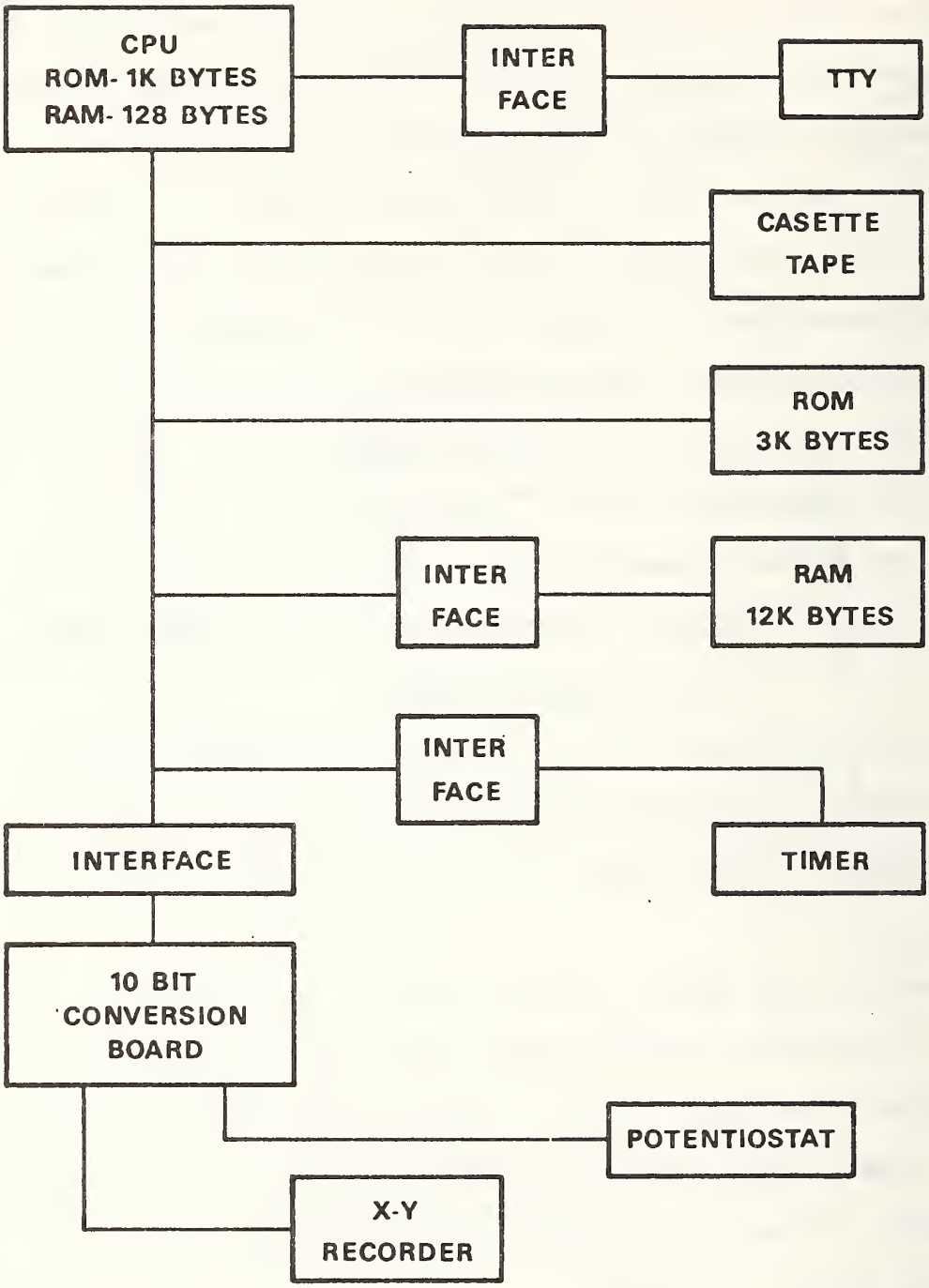

Figure 8. Configuration of the data conversion portion of the system. Direction of data flow is shown by the arrows. Alternative methods are indicated by dashed lines.

that the maximum frequency of a full scale triangular wave out of the converter is 25 Hz. To allow for this, a multiplexer has been added, and when desired the digital-to-analog output DAC #1 may be fed to a voltage controlled oscillator (max. freq. 3 MHz). Digital-to-analog converter #2 is used when a plot of log of the current vs. input potential is desired.

Control of the output wave shape is achieved by suitable programming. The most common output is in the form of a stepped triangular scan with the residence time at each point preselected by the operator. This enables determination of Tafel slopes by utilizing long step-delay periods and allows dynamic scans by using short periods. Other wave shapes can be obtained by entering the appropriate program.

The analog-to-digital converter (ADC) has an input range of -5 to +5 volts and a conversion frequency of approximately 40 kHz. It is a tracking type of converter [8], which means it is on all the time and rapidly tracks the input, except when halted by the computer to output data. The input voltage may be either direct or through a voltage divider, which effectively doubles the input range but reduces the resolution.

Operation of the System

Operation of the system will be described by referring to Fig. 9, which is a typical printout of a run, and to Fig. 8.

At initiation of the program the CPU prints out an identifier (DATA-TAKING-RAMP) and then requests an operator input (DELAY RATE). Upon receiving this, the CPU sets the basic timing frequency of the interval timer. The CPU then requests the number of basic counts (DELAY COUNT) and sets the interval timer's counter. It then requests the number of times the operator wishes to go up and down (SWEEPS), the step

```
*G
DATA-TAKING RAMP.

DELAY RATE
>0                          10 SEC PER COUNT  }
DELAY COUNT                                   }  5 MIN/SCANNED POINT
>30                         30 COUNTS         }
# SWEEPS
>1
STEP MVLT
>100                                  MATERIAL:        PLATINUM
HI/LOW MVLTS                          ELECTROLYTE:     1 M PHOSPHORIC ACID
>1000                                 REFERENCE:       CALOMEL
                                      2ND AND THIRD
>-310                                    COLUMNS:      5000 MV = 1MA

IS
  1000 -   70 -   70
   900 -   70 -   70
   800 -   90 -   90
   700 -   50 -   50
   600 -   90 -   90
   500 -   90 -   90
   400 -  110 -  110
   300 -   90 -   90
   200 -   70 -   70
   100 -   70 -   70
       -  110 -  110
-  100 -   70 -   70
-  200 -   90 -   90
-  300 - 1650 - 1650

IS
-  300 - 1330 - 1330
-  200 -  130 -  130
-  100 -  110 -  110
       -   90 -   90
   100 -   90 -   90
   200 -   90 -   90
   300 -   70 -   70
   400 -   70 -   70
   500 -   70 -   70
   600 -   90 -   90
   700 -   70 -   70
   800 -   30 -   30
   900 -   50 -   50
  1000 -   90 -   90
```

Figure 9. Sample print-out from a measurement using the microprocessor controlled electrochemical system.

size and the limits (HI/LOW). After receiving this information, the CPU loads the parameters in the program and then signals that it is waiting for a start (!). When ready the operator types an S and the experiment begins.

The CPU loads the upper limit value into DAC #1, outputs the analog voltage to the input of the potentiostat and starts the timer. When the interval is over, the timer signals the CPU which reads the ADC, checks the point against the lower limit, substracts the step size from the upper limit value and then outputs the next point. If the interval is long enough (>1.5 seconds), the CPU outputs the data. If too short, the CPU stores the data for subsequent output. The data format used is: the first column is the potential input to potentiostat, the second column is the output current of the potentiostat, and the third column is either the log of the current, or when that is not required, a repeat of column 2. When the lower limit is reached, the CPU asks for another command to sweep up.

In addition to the printout, the X-Y recorder normally reads the outputs of the potentiostat (voltage and current). If desired, these may be digitally plotted by the CPU, allowing plots of the log of the current vs. input potential.

Future Plans (Hardware)

As indicated earlier, provision has been made for addition of a modem and high speed parallel output. These are to be implemented very soon. Also, a programmable gain amplifier to increase the resolution of the ADC is being designed. It would be preferable to increase the resolution of the ADC and DAC's by purchase of higher resolution devices

(12 bit or greater), and if funds allow, this is the route we will take. Initial design of interfaces for other types of measurements (mainly ac) is underway. Memory enlargement is also desirable, both in form of more RAM and by the addition of mass storage such as floppy-disc memory. As mentioned earlier, the PROM board must be finished, and if possible, the additional PROM's to fill it to its capabilities must be purchased. The addition of a good digital plotter is also suggested.

Present plans also indicate that (with proper shielding) it would be possible to mount the entire existing unit within the potentiostat housing, and this may well be implemented.

Future Plans (Software)

Of first priority is the completion of the necessary programs for successful operation of the existing system [9]. The addition of an assembler and a higher-level programming language, such as BASIC or FORTRAN, either resident in the system or time shared on a large computer is needed. Although machine-language programming is more economical in terms of memory space needed, it is more wasteful by far of the programmer's time.

In view of the need for operation of the system by more than one individual; a larger body of non-volatile (PROM) programs in the unit is desirable. Such a mode of operation requires that these resident these are accessible by simple commands and are forgiving of improperly operated switches, etc.

Conclusion

A system has been built that, for a relatively low cost, allows electrochemical experiments to be performed under computer control. A limited amount of data analysis can be performed *in situ*, and the results

can be communicated to a central facility for complete analysis. The system provides for keyboard operational control and outputs both digital data and analog plots.

2.2 High Temperature Solid Electrolytes

Introduction

Oxide solid solutions having a defective fluorite structure and based on ZrO_2, CeO_2 and ThO_2, doped with CaO, Y_2O_3 or the trivalent rare earth oxides, have high oxygen-ion mobilities relative to the pure constituent oxides. The high oxygen-ion mobilities make these oxide solid solutions potentially useful solid electrolytes for high temperature fuel cells. The high oxygen-ion mobility results from the large concentration of oxygen vacancies introduced into the oxygen sublattice of the host oxide, about 5 to 15 mole % of dopant may be added depending upon the oxide system.

ZrO_2-based solid solutions have been used as electrolytes for high-temperature electromotive force measurements since the mid-1930's [10,11], and ThO_2-based electrolytes, since 1957 [12]. ZrO_2-based electrolytes have been studied for fuel cell applications principally at Westinghouse and G.E. in the United States, and elsewhere in France, Germany and the Soviet Union. Recent results [13,14] on CeO_2:Ln_2O_3, where Ln represents a variety of lanthanide ion or Y^{3+}, have revealed oxygen-ion conductivities essentially equivalent to that of ZrO_2:CaO but at temperatures about 200 °C lower. Thus, fuel cells using a CeO_2-based electrolyte might operate at about 800 °C as compared to one with a ZrO_2-based electrolyte which would require 1000 °C. However, CeO_2-based electrolytes begin to show appreciable electronic conduction at higher oxygen partial pressures than do the ZrO_2-electrolytes; for example, one-half of the electrical conductivity is electronic in $(CeO_2)_{0.95}(Y_2O_3)_{0.05}$ at $P_{O_2} = 10^{-14}$ atm

($\sim 10^{-19}$ Pa) for t = 800 °C, whereas for ZrO_2:CaO, $P_{O_2} = 2.5 \times 10^{-31}$ atm (2.5×10^{-36} Pa) for t = 1000 °C [15].

At the high oxygen vacancy concentrations present in these electrolytes, the oxygen vacancies are probably nearly all associated with the dopant cations [16]. If these electrolytes undergo prolonged anneals at moderate temperatures (<1000 °C), the oxygen vacancies, and perhaps to a lesser extent, the dopant cations, may order into a structure coherent with the fluorite structure of the host oxide. Formally, in terms of a coherent structure, the vacancies no longer exist. In actual consequence, the ionic conductivity of the electrolyte may decrease (resistance may increase) because the vacancies, relative to the fluorite structure, must then move cooperatively.

The existence of coherent structures is well documented for ZrO_2-based solid solutions [17-24]. Coherent structures in CeO_2-based solid solutions have not been identified.

Carter and Roth [21] found that the increase in resistance of calcia stabilized zirconia (CSZ) when annealed at <1000 °C was associated with the formation of coherent structures, observed as superstructure in neutron and x-ray diffraction. This "aging" of CSZ could be reversed ("deaged") by annealing at 1400 °C. In a high temperature fuel cell, aging of the electrolyte would reduce the efficiency of the cell.

A second aging process which may alter the long-term performance of a high temperature fuel cell electrolyte is the redistribution of the dopant cations along the grain boundaries. Relative to the lattice, the dopant cations appear as negative charges. Thus, they can be expected to migrate under the influence of an applied field. Although the mobility

of these cations within the interior of the grain is negligibly small for practical purposes, their mobility in the grain boundaries can be significant. For example, from the tracer diffusion measurements for Ca^{2+} ions in CSZ [25], the time required for Ca^{2+} ions to cross a 20 μm thick electrolyte film with a potential difference of 0.8 V is on the order of hundreds of years. On the other hand, the same tracer diffusion study showed that migration of Ca^{2+} ions in the grain boundaries is perhaps 1000 times larger at 1800 °C than the bulk diffusion rate, a ratio that would be expected to be even larger at lower temperatures. Hence, migration of the dopant ions along grain boundary paths over significant distances during times of the order of a year or less can be expected in all of the fluorite-structure oxides of current interest as solid electrolytes.

The migration of dopant ions along grain boundaries can be expected to result in at least three deleterious effects: (1) a build-up of a resistive layer at either electrolyte boundary, (2) a build-up of a space charge at the electrodes resulting effectively in an overvoltage, and (3) a possible interference with the electrode reaction due to a change in electrolyte composition at the electrolyte-electrode boundaries.

The NBS study of high-temperature solid electrolytes was initiated this year to investigate the possible aging of CeO_2-based electrolyte materials. Experiments were designed to study the aging of these materials both by ordering of the vacancies and by migration of the dopant cations. The principal research tool to be employed in the study will be the measurement of ac impedance, which yields values for the bulk and grain boundary conductances. Specimens will be annealed for a variety of

times and conditions. These measurements will be combined with structural studies and measurements of other physical parameters.

Design of the Experiments

With the help of Dr. John Mandel, experiments were designed to examine the rate of aging of solid electrolyte materials for various conditions of composition, temperature, oxygen partial pressure and current density. For each condition at least one replicate experiment will be performed to establish the uncontrolled variation in the experiments. With the exception of oxygen partial pressure, the range of the sampling for each condition will include the probable condition under which a ceramic electrolyte of such material would be used. The conditions to be sampled are summarized in Tables 4 and 5. The materials selected for study are hot-pressed CeO_2:Y_2O_3 and CeO_2:Gd_2O_3 solid solutions, with the Y_2O_3 and Gd_2O_3 in the range of 5 to 18 m/o.

Table 4 presents the conditions selected for the ordering experiment. In this experiment specimens will be extracted after the prescribed annealing times, electrodes then will be applied to the specimens and ac impedance measurements will be made. If ordering, for example, the formation of coherent structures, occurs as a result of the annealing, the bulk resistance is expected to increase; minor changes in the geometric capacitance may also occur. The ordering experiment will be performed under zero current conditions.

Table 5 presents the conditions for the migration experiment. In this experiment a DC electric field will be imposed on one set of specimens so that a constant current through the specimens will be maintained; a second set of specimens will be maintained under a field-free (zero

Table 4. Proposed ordering experiment.

Specimens: CeO_2 + 10, 20 or 30 atom % $YO_{1.5}$ or $GdO_{1.5}$;
40 specimens of each composition

Oxygen partial pressure: $\sim 10^{-4}$ atm

Temperature: 500, 700, 900, 1100°C

Sampling times: 1, 2, 4, 8, 16, and 32 weeks

Procedure: Two specimens of each composition removed from each furnace at the end of each annealing period; for electrical measurements; specimens not returned to furnaces after electrical measurements are made.

Expected results: If ordering of the oxygen vacancies occurs, a decrease in the ionic conductivity with increased ordering is expected. Specimens with significant changes in electrical properties will be examined by other techniques.

Table 5. Proposed migration experiment.

Specimens:	CeO_2 + 10 or 20 atom % $YO_{1.5}$ or $GdO_{1.5}$; 6 specimens of each composition
Oxygen partial pressure:	∿0.2 atm
Temperature:	Max. temperature allowed by stability of Pt electrodes, perhaps ∿900°C.
Current density:	∿1 A/cm^2 and 0 A/cm^2 (blank).
Procedure:	Periodic electrical measurements will be made on the specimens without removing the specimens from the furnace.
Expected results:	Migration of the dopant cation (Y or Gd) as a small secondary ionic current is expected to deplete the dopant cations at the cathode and to enhance the concentration at the anode, thus changing the electrical characteristics of the specimen.

current) condition. The resistance of both sets of specimens will be measured during the anneal without removal of the specimens from the furnace.

The experiments as designed impose a number of requirements. First, a large number of specimens is required: between 50 and 60 at each of the compositions, including "blanks" which will not be annealed. Second, annealing of 30 specimens at a single temperature in the ordering experiment places two stringent constraints on the furnace: a large isothermal zone, and the ability to insert and remove specimens with little perturbation of the specimens in the furnace. Two transparent furnaces were obtained for the ordering anneals at 500 and 700 °C. Two furnaces were built for the anneals at 900 and 1100 °C; these are described in the next section.

To minimize complications in the measured ac impedance due to grain boundaries and pores in the specimens, and to avoid changes in the electrical characteristics of specimens due to further densification during the anneals, hot-pressing was selected as the technique for preparing specimens of nearly full density. Sintered specimens also have been prepared to establish the hot-pressing conditions and to obtain some preliminary samples for ac-impedance measurements. Details are given in the section on electrolyte materials.

High Temperature Facility

A laboratory was remodeled to provide the high temperature facility for the ordering and the migration experiments. To allow working space and ease of access to the furnaces, a central island was installed which

consists of modular, counter-height relay racks to hold the controllers and power supplies for the furnaces. Connection of the controllers and power supplies is now in progress; the countertop has yet to be delivered and installed. The five furnaces required for the experiment will be emplaced on the island when it is completed.

Transparent furnaces were selected for the low-temperature ordering anneals because these furnaces have a very flat temperature profile through the hot-zone and because they permit observation of the specimens. These furnaces can be operated at temperatures up to 1000 °C.

For the high-temperature ordering anneals conventional resistance furnaces with three independent heat zones were constructed. A schematic of these furnaces is shown in Fig. 10. The main heater and the two end heaters are independently regulated. These furnaces can be operated up to 1200 °C. For the migration experiment a Pt-Rh wound multiple-zone tube furnace is available.

The system for the distribution of power to a three-zone furnace was suggested by Mr. Harry Parker; a schematic of the system is shown in Fig. 11. The output of a thermocouple in the main-heater zone is fed to a controller which regulates the total power to the furnace. The output of the power supply regulated by the controller energizes the primary of a transformer. Power for the main heater is obtained from the full secondary of the transformer; power for the two end heaters is taken from the two halves of the secondary via variable autotransformers.

Electrolyte Materials

a. Preparation and Characterization

Initially specimens were prepared by mechanically mixing the oxide powders; forming the powder into disks or billets; isostatically pressing

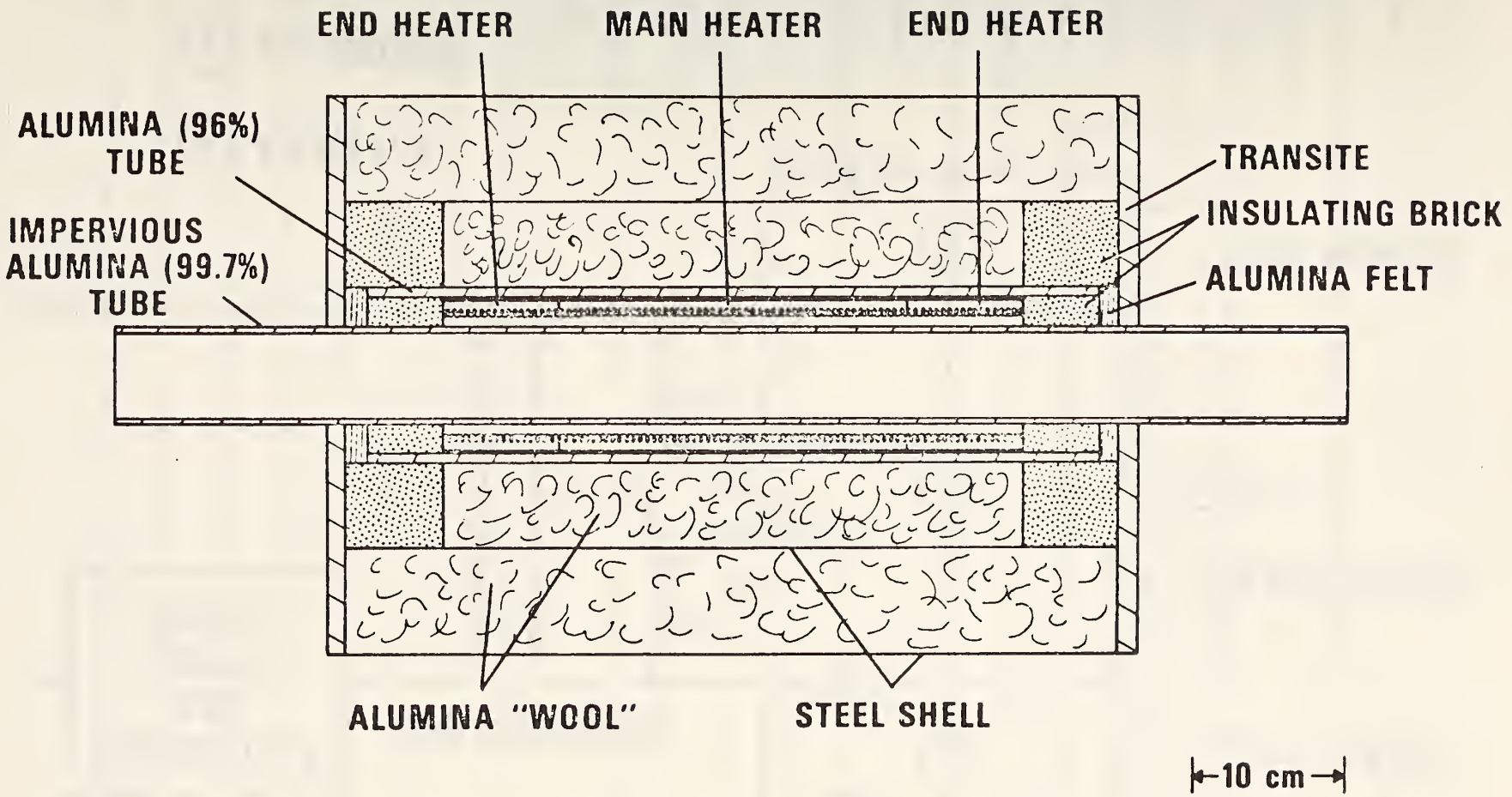

Figure 10. Three-zone resistance furnace.

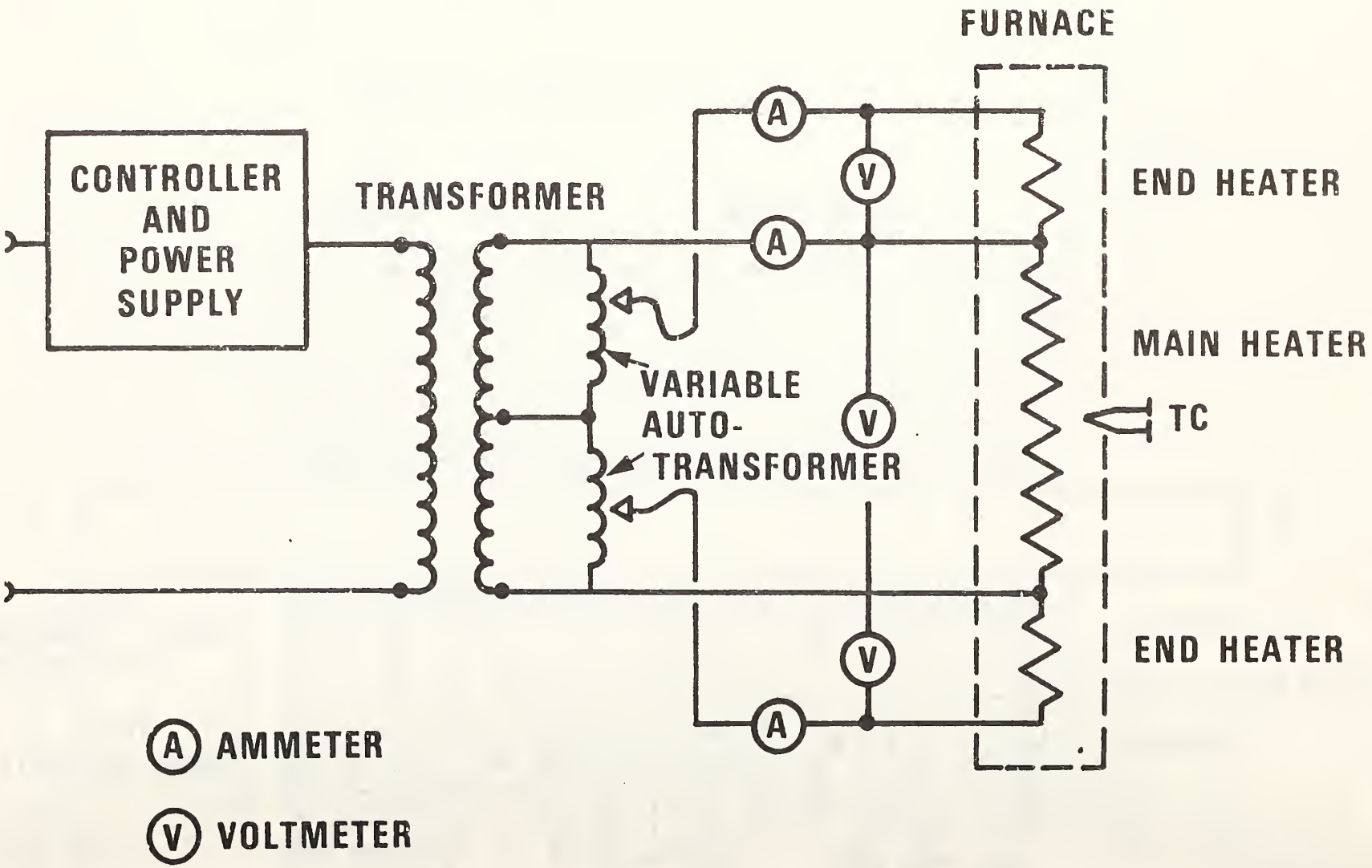

Figure 11. Power distribution system for the three-zone resistance furnace.

to achieve a high, uniform green density; and sintering or hot-pressing. Mechanical mixing of the oxide powders was selected on the basis that it would minimize the introduction of impurities during the preparation of the specimens.

Densities and estimated porosities of sintered and hot-pressed specimens are given in Table 6 along with composition, calcination conditions for the powder, and sintering or hot-pressing conditions. Two densities are given: the bulk density for which the relevant volume includes both the open and closed pores, and the "intrinsic" density for which the volume includes only the closed pores. The bulk density is obtained from the mass of the specimen and the geometric volume, if the specimen has a regular shape, or from a buoyancy measurement in mercury. The intrinsic density is obtained from a buoyancy measurement using a fluorocarbon liquid which penetrates the open pores of the specimen. The maximum bulk density obtained by sintering the mechanically mixed oxide powders was 91% of theoretical; and by hot-pressing, 93 to 94% of theoretical.

Calcination of the mixed powders to homogenize them prior to sintering reduced the sinterability of the powder.

Densities of about 93% of theoretical have been reported as routine for sintered CeO_2:Y_2O_3 specimens [26]. Also, an X-ray diffraction study of the hot-pressed material showed the presence of the CeO_2 and the Y_2O_3 phases, and not solely the solid-solution phase. Consequently, it appeared that a chemical preparation of the mixed oxide powder was required to achieve a higher density and to obtain a homogeneous solid solution.

Table 6. Density and porosity of sintered and hot-pressed specimens.

Composition $CeO_2/YO_{1.5}$ atom %	Calcination conditions °C	hrs	Sintering or hot-pressing conditions °C	hrs	Bulk density[a] % theor.	Intrinsic density[a] % theor.	Open porosity % vol.	Closed porosity % vol.
70/30	1400	14	1600	1½	72±3	86	16	12
			1400	14				
90/10	1500	9	1600	15½	84	87	3.4	13
			1500	2				
			1300	1				
70/30	1500	9	1600	15½	74	87	15	11
			1500	2				
			1300	1				
80/20	1400	2	1600	2	88±3	91±2	3.3	8.7
			1500	14				
80/20	1300	4	1600	2	91	94	3.2	5.8
			1500	14				
90/10	none		1560	4	79	82±1	3.7	17
			1420	16				
70/30	none		1560	4	85	88	3.4	12
			1420	16				
90/10	1200	9	1350	3/4	92.8[b]	93.4[b]	0.64	6.56
			28 MPa		93.6[c]	94.2[c]	0.64	5.76

a. Theoretical densities (g/cm^3): 10 a/o $YO_{1.5}$, 6.98; 20 a/o $YO_{1.5}$, 6.74; 30 a/o $YO_{1.5}$, 6.51.
b. Based on the theoretical density of the solid solution, see footnote a.
c. Based on the theoretical density of the fully dense mixture, 6.92 g/cm^3.

Micrographic examination, Fig. 12 and 13, also showed a two-phase material. Coarse grains (gray in Fig. 12) are dispersed in a white, fine-grain matrix. The black areas are pullouts from the polishing and pores. In Fig. 13, etching of the specimen in a dilute mixture of nitric acid and hydrofluoric acid reveals the fine-grain structure of the matrix and the coarse grains of the second phase. The matrix is presumably ceria, and the coarse grains, yttria. A scanning electron microscopy (SEM) was used to examine the pullouts and pores in one specimen. Fig. 14 is a typical SEM micrograph of one of the pullouts on the surface of a hot-pressed specimen. Pores are evident in the bottoms of the pullouts.

Before embarking on a, perhaps lengthy, chemical preparation of the CeO_2:Y_2O_3 powder, chemical analyses of the possible starting materials was obtained as work on CeO_2:Ta_2O_5 at NBS had found sodium as a major contaminant in the CeO_2 used in that work. The mass fractions of impurities in some mixed powders, in a cerous nitrate and a cerous carbonate are given in Table 7.

The first chemical technique tried in this work used 6N sulfuric acid containing some hydrogen peroxide to effect the dissolution of the CeO_2. This technique required several subsequent dissolutions in nitric acid, followed each time by precipitation with ammonium hydroxide, to remove the sulfate. In addition, the initial dissolution of the CeO_2 by the sulfuric acid was very slow. More recently, the use of concentrated nitric acid containing a few drops of hydrofluoric acid was suggested to us as a solvent for CeO_2 [27]; this reagent has been found to work successfully for our CeO_2 powders. To reduce the contamination in the

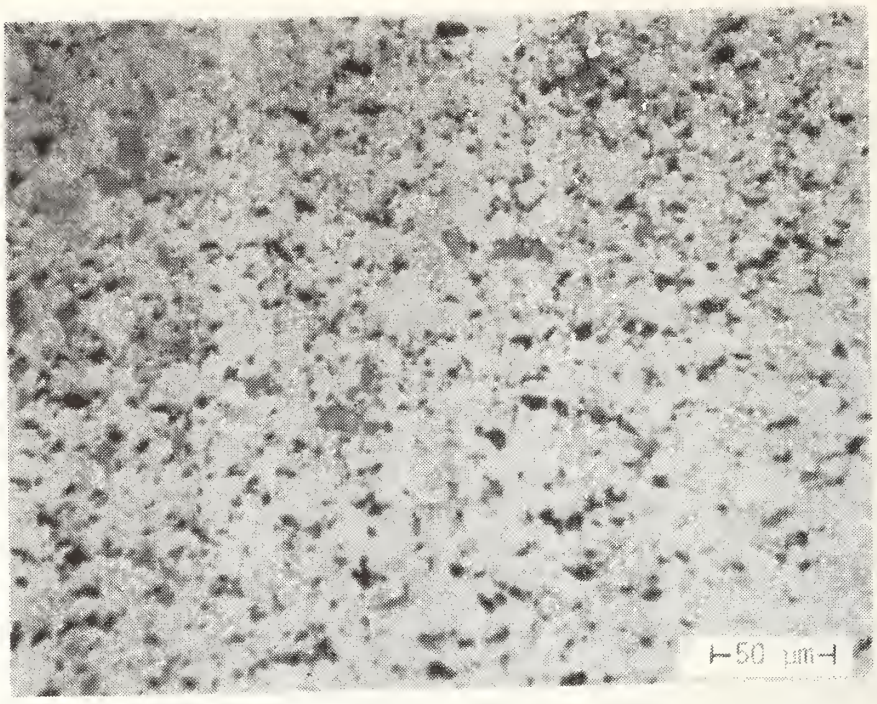

Figure 12. Optical micrograph (320X) of hot-pressed CeO_2:Y_2O_3. Oxide powders were mechanically mixed. A duplex structure of fine, "white" grains and coarse, "gray" grains is present; black regions are pullouts produced by polishing and pores.

Figure 13. Optical micrograph (800X) of hot-pressed CeO_2:Y_2O_3; oxide powders were mechanically mixed prior to hot-pressing. The specimen was etched in dilute nitric acid/hydrofluoric acid to reveal the grain boundaries.

Table 7. Impurities in CeO_2:Y_2O_3, $Ce_2(NO_3)_3$ and $Ce_2(CO_3)_3$ powders.

Sample	Na, mg/g	μg/g K	Ca	Mg	Al	Fe	Si
CeO_2:Y_2O_3--99.99% oxide powders mechanically mixed	0.030	7.7	19.4	3.7	31	27	<5
CeO_2:Y_2O_3--mixed powder chemically prepared from 99.99% oxides	0.047	5.6	12.4	8.7	55	43	<5
CeO_2:Y_2O_3--mechanically mixed powders hot-pressed, followed by grinding in an alumina mortar	0.028	4.9	22.6	4.3	108	19	<5
$Ce_2(NO_3)_3$[a]	0.086	0.5	13.5	78.6	7	43	<5
$Ce_2(CO_3)_3$[a]	5.91	3.7	300	10.7	30	42	<5

[a] Commercially prepared.

chemical preparation, the glass labware has been replaced by polyethylene items. By dissolving the high-purity oxides in nitric acid, coprecipitating from the mixed solutions and avoiding sources of sodium impurity, homogeneous mixed oxide powders with purities comparable to that of the starting material are to be expected.

b. Annealing Experiment

Three of the hot-pressed specimens were annealed at 1400, 1500 and 1550 °C, respectively. The total annealing times were 100 hours at 1400, 48 hours at 1500 and 120 hours at 1550 °C. The two-phase appearance was not distinguishable after 48 hours at 1400 °C; however, this may have been due in part to the roughening of the surface which occurred during the anneal. After 100 hours at 1400 °C, grains or crystallites resembling clusters of grapes had begun to develop. These grape-like clusters were even more evident after annealing at 1500 °C and at 1550 °C, see Fig. 15. The size of the clusters and their number increased with annealing temperature and time. These clusters may be the solid-solution phase. The three specimens have been repolished and will be examined by x-ray diffraction and by optical and electron microscopy.

Impedance Measurements

Our impedance measuring techniques have been improved markedly in three important aspects. We now have a furnace for use in making electrical measurements that has extended high temperature capability and improved gaseous environmental control. Our network analyzer system has extended the frequency range of our measurements and improved our resolution. We have developed sputtered Pt electrodes that exhibit high temperature stability.

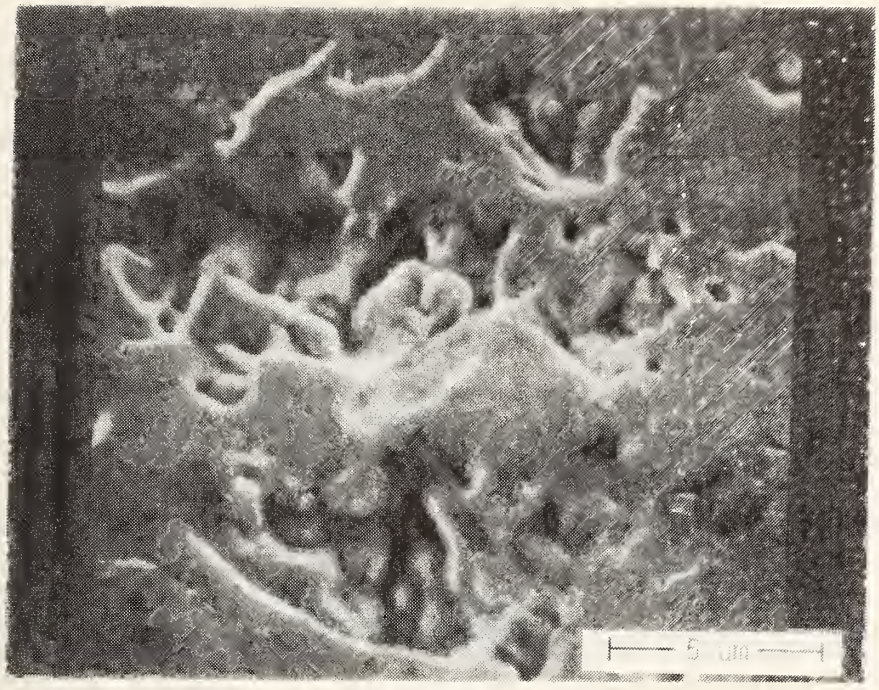

Figure 14. SEM micrograph (5600X) of pullouts and pores in hot-pressed CeO_2:Y_2O_3.

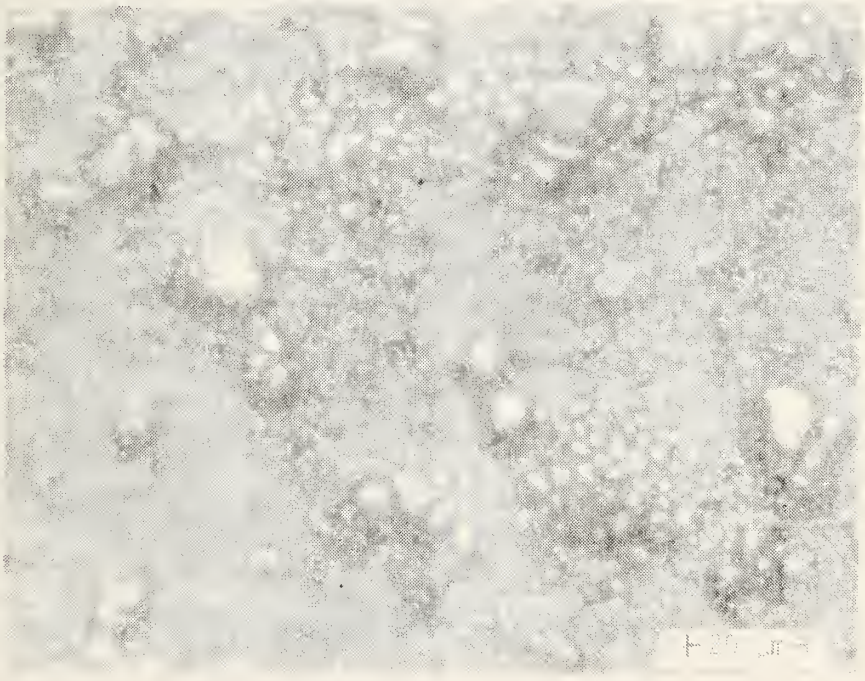

Figure 15. Optical micrograph (800X) of hot-pressed CeO_2:Y_2O_3 after an anneal of 120 hr. at 1550 °C in air. The specimen originally had a duplex structure of ceria and yttria grains. The specimen shows growth of new grains (grape-like clusters).

We modified an existing furnace so that electrical impedance measurements could be made with our network analyzer. This furnace was then operated satisfactorily at temperatures up to 800 °C, and it also has the potential of attaining somewhat higher temperatures. The gaseous environment of the specimen chamber of this furnace can be controlled either in a uniform way or by applying a differential partial pressure of O_2 across the specimen.

Using the network analyzer system provides an extended frequency range as compared to the time honored technique of using an ac-impedance bridge. The network analyzer sacrifices some resolution in the mid range of frequencies (1 kHz to 20 kHz), however, the extension of the low frequency limit to 10 Hz and the high frequency limit to 13 MHz makes it far more useful in sorting out multiple relaxation processes and other related phenomena. We presently operate the network analyzer system in a semiautomatic mode and data collection is about 5 to 10 times faster than using an ac bridge. Our system also offers the potential of even more rapid automatic operation with the addition of a programmable calculator and suitable interfacing equipment.

When a network analyzer is operated in an insertion loss mode, as we use it, then its operation bears some resemblance to an ac-bridge measurement technique. Fig. 16 shows schematically the circuit we use to measure an unknown complex impedance Z*. It was drawn in such a way as to show its resemblance to an ac bridge. The most fundamental difference is that a bridge is adjusted to a null output for each desired frequency, and a network analyzer just compares V_A^* with V_B^* and gives the result directly. From the circuit shown in Fig. 16 Z* can be written as:

$$Z^* = 100 \left[\frac{E_A^*}{E_B^*} - 1 \right] \tag{1}$$

where E_A^* and E_B^* are complex electromotive forces (voltages). Since the voltages vary sinusoidally then they can be expressed as:

$$E_A^* = E_A e^{j\omega\tau}$$

$$E_B^* = E_B e^{j(\omega\tau - \phi)}, \tag{2}$$

where ω = frequency, t = time and ϕ = phase shift between E_A^* and E_B^*. The unknown Z^* then becomes

$$Z^* = 100 \left[\frac{E_A}{E_B} e^{j\phi} - 1 \right]. \tag{3}$$

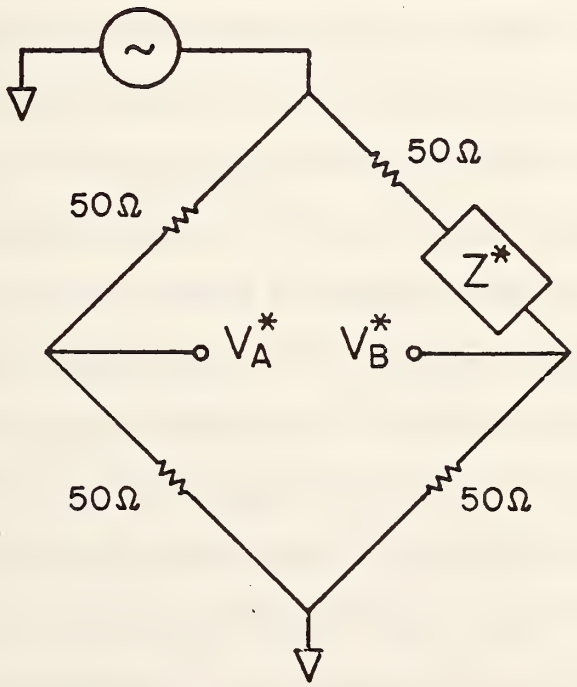

Figure 16. Schematic diagram of the measuring circuit for a network analyzer.

Second, the surface of the specimens was much too rough and(or) porous for the film to remain continuous. As our preparation of specimens improved and we achieved higher density, then the ground and polished surfaces were capable of being electroded with sputtered Pt that would withstand temperatures of at least 800 °C in N_2.

Impedance Data Analysis

We developed computer programs for data analysis using a Hewlett Packard 9830A progammable desktop calculator with a plotter attachment. For each measurement frequency the network analyzer displays the voltage ratio E_A/E_B (in dB) and the phase shift ϕ (in degrees) on a pair of L.E.D. readouts. A set of frequencies is then scanned and the data pairs are recorded in a logbook for later manual key board entry on the HP 9830A. When entered, the data is formatted, and then it is stored on magnetic tape cassettes. When the data are recalled for analysis, the impedance, Z*, is calculated from eq. (3). The admittance, Y*, is then easily calculated as the reciprocal of the impedance, $Z^* = 1/Y^*$.

Once these fundamental properties are obtained, then various graphical displays can be easily generated on the plotter peripheral of the HP 9830A. The complex impedance, Z*, or admittance Y* can be plotted with either or both variables raised to any arbitrary power. Either the real or imaginary parts of these complex quantities may be plotted versus frequency or log (frequency) and again these may be raised to any arbitrary power. This is most useful when attempting to sort out diffusional properties from relaxational ones. Diffusion-controlled electrical processes involve time raised to the 1/2 power, whereas,

single relaxation phenomena involve integer powers. When there are phenomena with distributions of relaxation times then the appropriate powers of dependence lie somewhere in between 1/2 and 1.

We use a linear least-square fitting procedure with 2 parameters in several ways. If the imaginary part of the impedance, Y*, is plotted against frequncy, ω, then at high frequency a linear dependence would indicate a capacitive effect is dominant. Fitting this linear portion would give the value of the capacitance as the slope because the admittance, Y*, for a pure capacitor is equal to ωC. If the complex impedance plot, Y*, has a linear region with a slope of unity, then it can be easily found by this procedure. This could indicate the presence of a diffusional impedance mechanism and can easily be verified by separately plotting the real and imaginary parts versus $\omega^{+1/2}$. A linear dependence here would confirm this, and allow an estimate of the diffusional impedance constant, σ, by fitting the slope of the linear portion.

In representing relaxational processes the model equivalent circuits are composed of resistors and capacitors. For the case of a single relaxation mechanism there is just one capacitor and one resistor, and for the case of a distribution of relaxation processes there is some combination of these circuit elements. The complex impedance of a single resistor and capacitor connected in parallel gives rise to a circular arc that passes through the origin with its center lying on the real axis. Multiple relaxation processes add up in such a way that either the center then falls below the real axis, or if the time constants of the processes are sufficiently different then the arcs become a series of "bumps" connected together. A circular-arc least-squares fitting procedure was developed in order to extract the parameters for

an equivalent circuit. A single well-defined arc can be characterized directly when it appears as the most prominent feature in the data. However, in certain instances the data can be "corrected" by subtracting frequency dependent capacitance effects as shown below in the next section.

Impedance Data Interpretation

Impedance measurements as a function of frequency and temperature, and in the presence of atmosphere composed of tank N_2 or O_2, have been made on several sintered specimens of Y-doped CeO_2. These specimens are somewhat porous, and the electrodes are somewhat irregular in outline. No attempt has yet been made to reduce the data to intrinsic material properties.

Figure 17 shows typical data taken on the same specimen at several temperatures in the same atmosphere. Here the complex impedance is plotted in the complex plane. Physical and chemical processes normally become faster as the temperature rises, while the frequencies available for measurement, and therefore the region of the time scale sampled, remain fixed. The result is that the "window" available to us to view the relative time scale moves toward the slower, lower-frequency processes as the temperature rises. This effect is clearly observable in Fig. 17, where the data appear to move toward the low-frequency (right-hand) side of the impedance diagram.

Within the portion of the time scale so far explored using the frequencies (10 Hz to 13 MHz) and temperatures (22 °C to 600 °C) available, the impedance plots exhibit two major arcs. At high frequencies, and

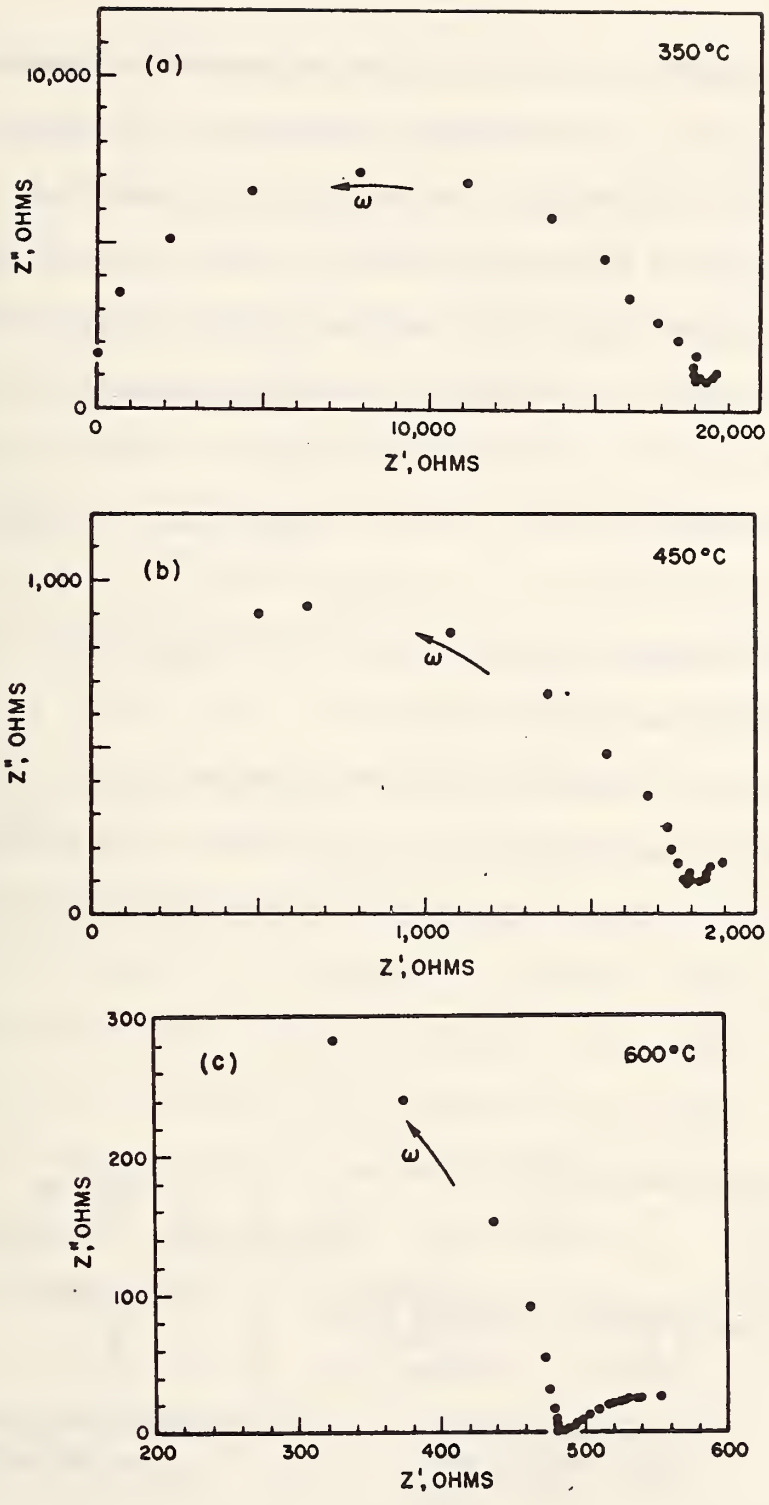

Figure 17. Impedance plotted in the complex plane for a sintered specimen (bulk density 85% of theoretical) of $Ce_{0.8}Y_{0.2}O_{1.9}$ at three temperatures shown.

low temperatures, there is a distorted arc independent of whether the atmosphere is O_2 or N_2, and therefore probably due to conduction processes in the bulk of the specimen, not involving electrode reactions. The distorted shape of this arc suggests that it is the result of the superposition of several processes, arising perhaps from the combined effects of the geometric capacitance, internal inhomogeneities such as grain boundaries, and the conductance of regions of "good" material between the inhomogeneities [28]. At low frequencies, and high temperatures, there is an additional arc, depressed below the real axis, details of which appear to depend upon the nature of the atmosphere. This arc probably arises from electrode effects.

It appears at this stage possible to represent these data by the equivalent circuit shown in Fig. 18. The part left of the dotted line arises from the bulk processes while that to the right represents electrode effects.

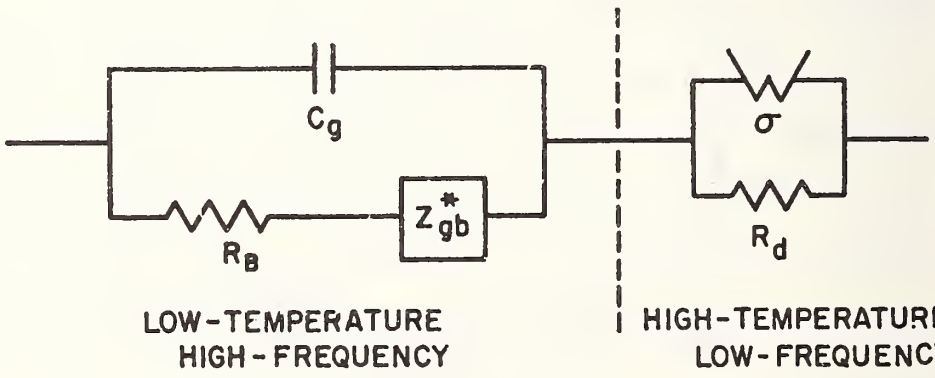

Figure 18. Equivalent circuit to represent impedance of polycrystalline $Ce_xY_{1-x}O_{2-x/2}$ specimens.

In the bulk part of the equivalent circuit as we interpret it at the moment, C' represents the geometric capacitance, R' the resistance of the "good" material between homogeneities, and Z^*_{gb} the impedance due to the inhomogeneities. The variable nature of these inhomogeneities has been accounted for by writing Z^*_{gb} as resulting from a Cole-Cole [29] distribution of relaxation times;

$$Z^*_{gb} = \frac{\Delta Z}{1 + (j\omega\tau)^n} \quad , \tag{4}$$

where ΔZ is the total resistance contributed by the inhomogeneities at zero frequency, ω is the circular frequency, τ is the most probable relaxation time, n is a parameter expressing the width of the distribution and j is equal to $\sqrt{-1}$. When n = 1, the distribution is a delta function. For n<1 the distribution broadens as n decreases.

A hand-waving rationale for treating the combined impedances of the inhomogeneities and the "good" material between in this fashion can be developed as follows. The bulk of the specimen can be thought of as a bundle of roughly identical chains, in parallel. Each chain consists of a string of inhomogeneities separated by "good" material. The inhomogeneities are thin, and must each be represented by a capacitor shunting a resistance, while the sections of "good" material are relatively long and contribute only resistances proportional to the length of the section. The corresponding capacitance has in fact been included in the geometric capacitance. When the impedance of this chain is calculated, the "good" material resistances combine in simple series fashion to give R', while

the impedances of the inhomogeneities combine in the series calculation as

$$Z^*_{gb} = \sum_i Z_i \approx \int_0^\infty Z(\tau)\, g(\tau)\, d\tau \quad , \tag{5}$$

where i is an index running over all inhomogeneities, $Z(\tau)$ is the impedance in this sequence corresponding to the range in relaxation times from τ to $\tau+d\tau$, and $g(\tau)$ is the distribution function for τ. With $g(\tau)$ given by the Cole-Cole distribution function, eq (5) reduces to eq (4).

Figure 19 shows an example of how the equivalent circuit fits the experimental data. The parameters of the equivalent circuit for this case are:

R' = 134 kΩ	ΔZ = 658 kΩ	n = 0.566
C' = 6.454 pF	τ = 8.87 μs	

They were obtained as follows. First, the very high frequency data were converted to admittances, Y*, and the imaginary part Y" plotted against ω, the circular frequency. The slope of the resulting line (Fig. 20) gives C' directly. The admittance values at all frequencies were then reduced by the contribution from this estimate of C', and inverted to yield the impedance of the $R'+Z^*_{gb}$ branch of the equivalent circuit. When plotted in the complex plane, this yielded a depressed arc that could be fitted by the least-squares techniques described above to a Cole-Cole equation. The results of this fit give the parameters of Z^*_{gb}. The high-frequency (left-hand) intercept of this arc on the real axis gives R'. With these parameters the overall impedance, shown as plus signs on Fig. 19, for the whole circuit was then calculated.

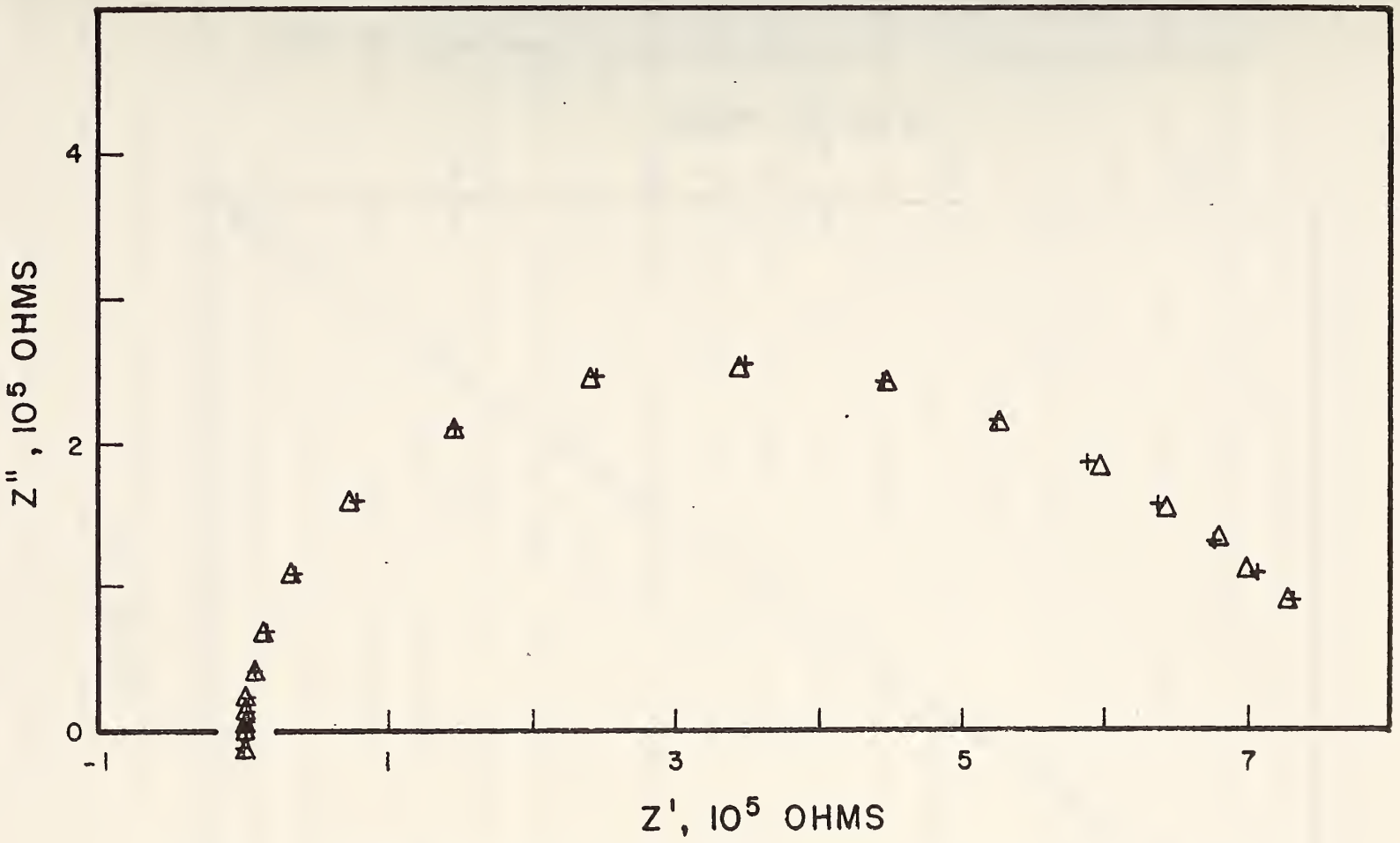

Figure 19. Complex impedance plot for $Ce_{0.8}Y_{0.2}O_{1.9}$ at 250 °C in O_2. Experimental points shown as △. Corresponding points calculated using the best fit of the equivalent circuit in Fig. 18, as discussed in the text, shown as +.

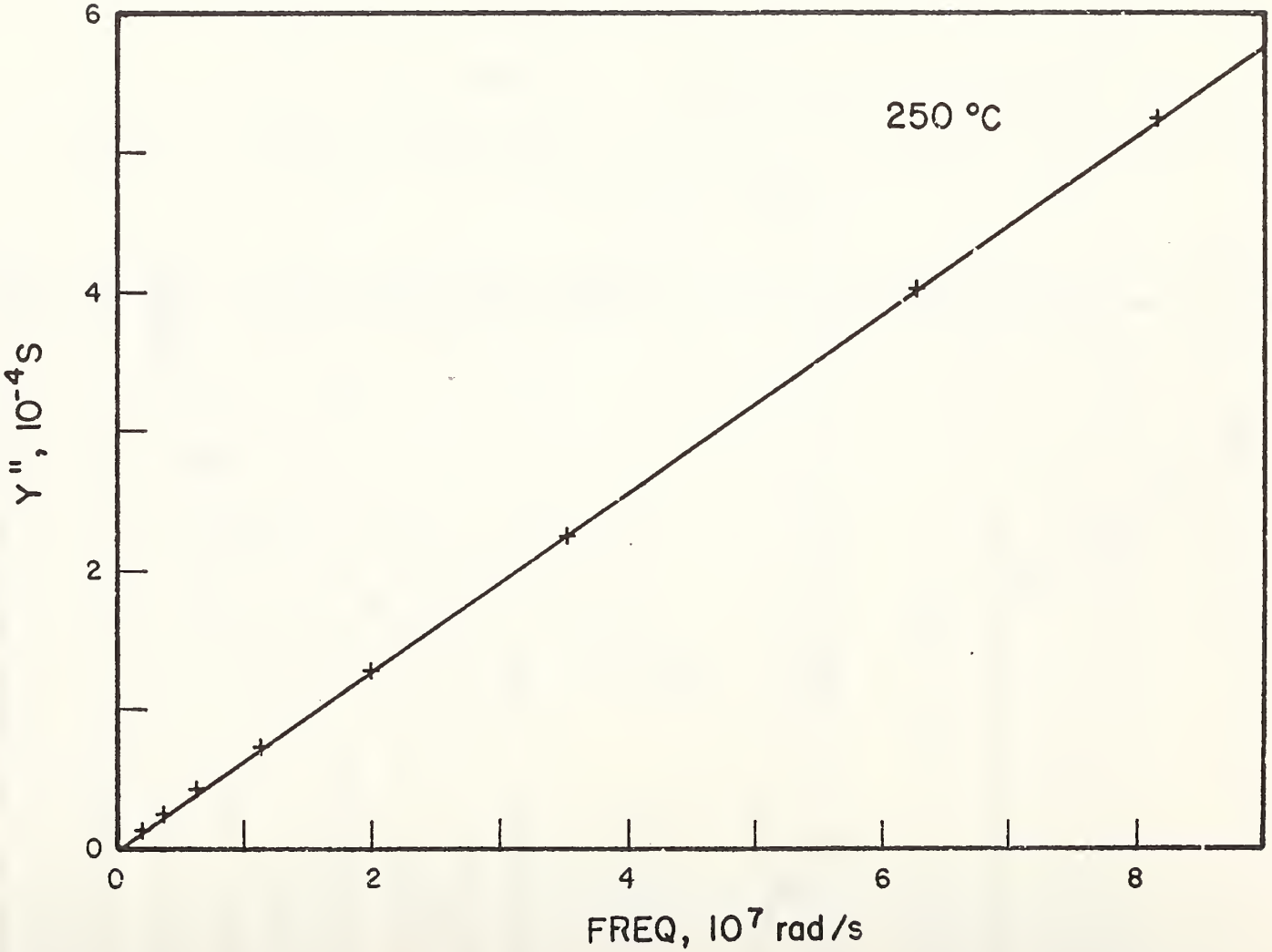

Figure 20. Dependence of the imaginary part Y', of the admittance of $Ce_{0.8}Y_{0.2}O_{1.9}$ at 250 °C in O_2 on circular frequency at the highest frequencies.

The fit appears to be quite good, and in particular offers the hope of estimating the true conductance of the "good" material, needed to monitor and assess the results of the degradation studies described above. The fitting procedure described is clumsy and, because of slow convergency, may not yield good estimates of the parameters in every case. For this reason, future work will include the development of a steepest-descents computer program to allow fitting of the whole equivalent circuit to all of the data simultaneously.

These techniques should be useful beyond the simple estimation of R', which in turn will yield the conductance of the "good" material between inhomogeneities. There is also, in Z^*_{gb}, information about the inhomogeneities themselves, if the model proves to be sound. The inhomogeneities may be grain boundaries, regions of a second phase, pores, and perhaps even extended defects or stacking faults. The technique could thus be used to guide efforts to develop optimum microstructures, or to monitor changes in microstructure during aging. Experiments are planned to try in the immediate future to prove the validity of the model.

At high temperatures and low frequencies an additional arc appears. At 600 °C in O_2, as shown in Fig. 21, the complex impedance at low frequencies is well fitted by a circular arc with center depressed below the real axis. The angle between the real axis and the line joining the left intercept of the arc on the real axis and the center of the arc is 44°. Fig. 22 shows that for these same data a very similar arc is exhibited by the complex admittance. If we identify the left intercept of this arc, in the impedance plot as R_t, the right intercept in the admittance plot as R_t^{-1}, the right intercept in the impedance plot as R_t+R_d, and the left intercept in the admittance plot as $(R_t+R_d)^{-1}$, then

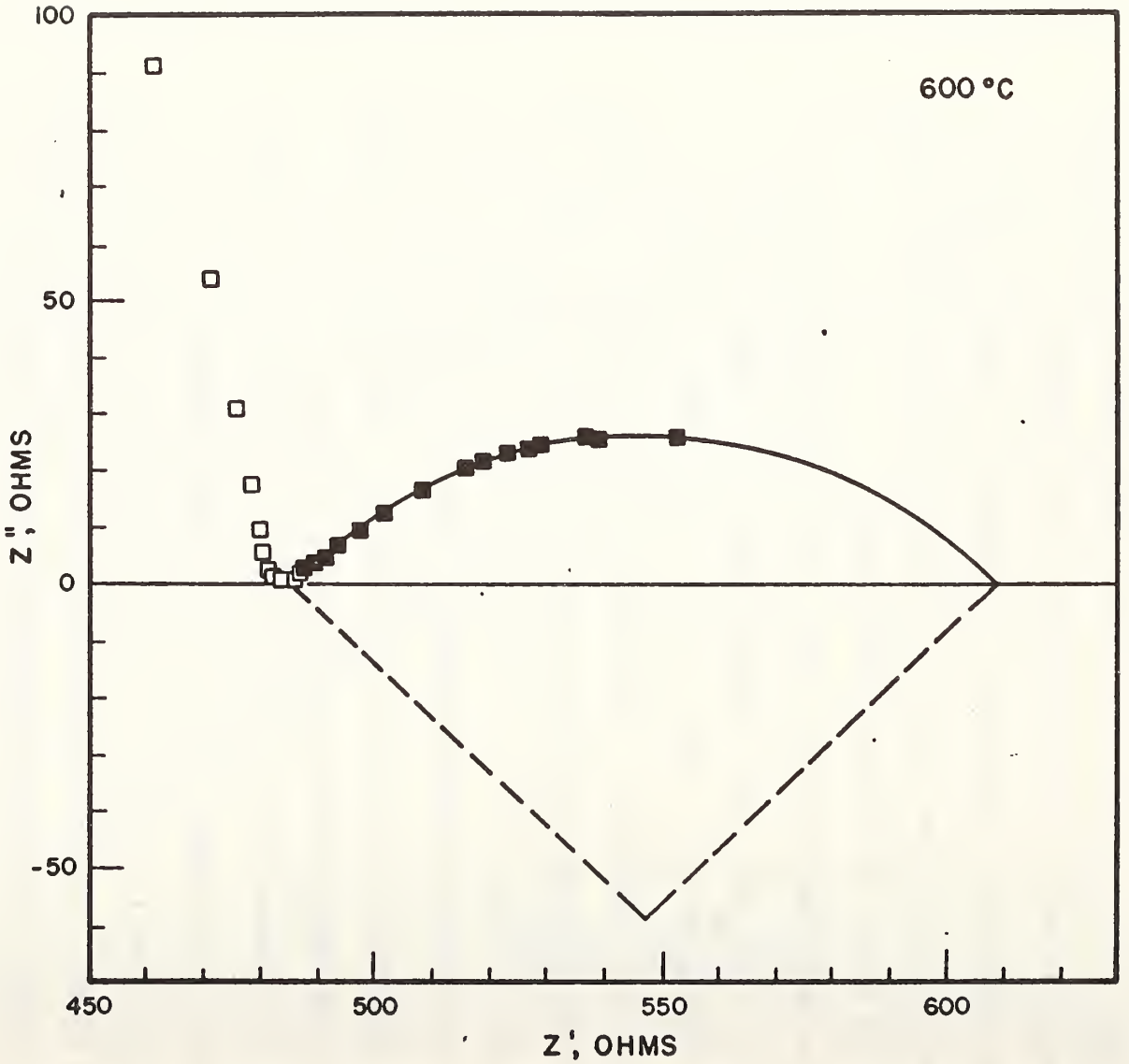

Figure 21. Complex impedance of sintered $Ce_{0.8}Y_{0.2}O_{1.9}$ at 600 °C in O_2.

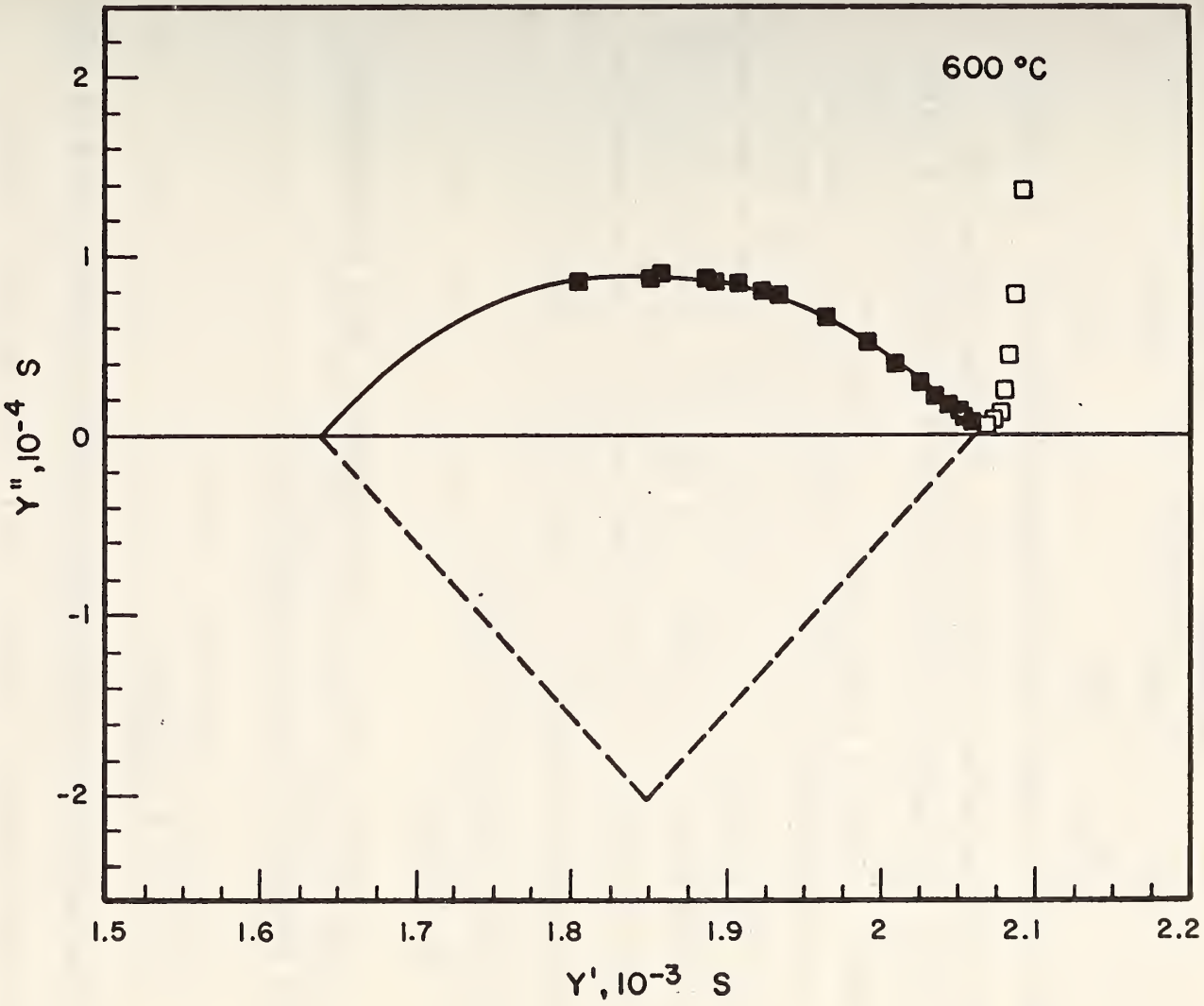

Figure 22. Complex admittance of sintered $Ce_{0.8}Y_{0.2}O_{1.9}$ at 600 °C in O_2.

the fits shown in Figs. 21 and 22 result in the following estimates for these parameters:

	Impedance,	Admittance,
R_t,Ω	486	485
R_t+R_d,Ω	609	610

These results suggest several alternate explanations. In the first the part of the equivalent circuit in Fig. 16 to the right of the dashed line is represented by Warburg impedance, representing a diffusional process, shunted by a resistance, R_d, representing the electrode process involving oxidation of O^{2-} ions and reduction of O_2, and exchange with the atmosphere. The diffusional process might be the storage of O_2 as solute in the Pt electrodes. At these low frequencies and high temperatures the bulk processes have been reduced to simple conduction, represented by the resistance R_t in series with the electrodes.

The Warburg impedance is given by

$$Z_W^* = \sigma(1-j)\omega^{-\frac{1}{2}} \tag{6}$$

where σ is the intensity factor of the impedance. Then the impedance of the entire equivalent circuit as described is

$$Z^* = R_t + \left(\frac{R_d}{1+(j\omega\tau)^{\frac{1}{2}}}\right) \tag{7}$$

which is the equation for an arc depressed below the real axis such that the left (high-frequency) intercept is R_t, the right (low-frequency) intercept is (R_t+R_d), and the angle between the real axis and the line joining the left intercept to the center of the arc is $\pi/4$.

The admittance of this whole equivalent circuit is the inverse of Z^* given by eq (7):

$$Y^* = (Z^*)^{-1} = R_t^{-1} - \frac{\Delta Y}{1+(j\omega\tau')^{\frac{1}{2}}}, \tag{8}$$

where

$$\Delta Y = R_t^{-1} - (R_t+R_d)^{-1} \tag{9}$$

$$\tau' = \left(\frac{R_t}{R_t+R_d}\right)^2 \tau.$$

This is the equation for an arc with left intercept given by $(R_t+R_d)^{-1}$, right intercept by R_t^{-1}, and the angle between the real axis and the line joining the right intercept to the center of the arc given by $\pi/4$. These descriptions for the behavior of eqs (8) and (9) appear to match very closely the descriptions of the data given above. Furthermore, the ratio of τ'/τ drawn from the fit of the equations to the experimental data is 0.71, where the ratio $[R_t/(R_t+R_d)]^2$ is 0.64, satisfactory agreement as called for by eq (9).

Essentially the same set of equations (7 and 8) can be arrived at in a somewhat more general format by replacing the Warburg impedance by an element consisting of a set of parallel admittances, each of which consists of a series resistor and capacitor, and which are distributed according to a Cole-Cole distribution. The admittance for this element is

$$Y^* = Y_\infty - \frac{Y_\infty}{1+(j\omega\tau)^n}, \tag{10}$$

where Y_∞ is the conductance of the element at infinite frequency. The

impedance corresponding to eq (10) is

$$Z^* = Y_\infty^{-1} \left\{ 1+[\tau^{-n}\mathrm{Cos}(\tfrac{n\pi}{2})]\omega^{-n} - j[\tau^{-n}\mathrm{Sin}(\tfrac{n\pi}{2})]\omega^{-n} \right\} \qquad (11)$$

which for $n = \frac{1}{2}$ reduces to a Warburg impedance in series with a resistance given by Y_∞^{-1}. This formulation could account for departures of the exponent from $\frac{1}{2}$.

This discussion has presented a model that can account for the data observed so far. One of the immediate tasks will be to devise and carry out experiments to test and refine this model, and to relate its parameters to properties of the materials measurable in other ways.

References

1. P. Stonehart and P. N. Ross, Electrochim. Acta, 21, 441 (1976).
2. Potentiostat and its Applications, J. A. Von Fraunhofer and C. H. Banks, Butterworth, (London, 1972).
3. Electronics, 49, No. 8, (1976); Special Issue on Microprocessors.
4. An Introduction to Microcomputers, A. Osborne and Associates, Inc., Berkeley, CA (1975).
5. M6800 Microcomputer System Design Data, Motorola, Inc. (1976).
6. M6800 Microprocessor Applications Manual, Motorola, Inc. (1975).
7. Analog-Digital Conversion Handbook, edited by D. H. Sheingold, Analog Devices, Inc., Norwood, MA. (1972).
8. A Low Cost, High Performance Tracking A/D Converter, Application Note AN-6, Precision Monolithics, Inc., Santa Clara, CA.
9. Software Design for Microprocessors, J. G. Webster and W. D. Simpson, Texas Instrument Learning Center, Dallas, TX (1976).
10. W. Schottky, Wiss. Veroff. Siemenswerke, 14, H2, 1 (1935).
11. E. Baur and H. Preis, Z. Elektrochem., 43, 727 (1937).
12. K. Kiukkola and C. Wagner, J. Electrochem. Soc., 104, 379 (1957).
13. H. L. Tuller and A. S. Nowick, J. Electrochem. Soc., 122, 255 (1975).
14. T. Kudo and H. Obayashi, J. Electrochem. Soc., 122, 142 (1975); 123, 415 (1976).
15. J. W. Patterson, E. C. Bogren and R. A. Rapp, J. Electrochem. Soc., 114, 752 (1967).

16. A. S. Nowick and D. S. Park, "Fluorite-Type Oxygen Conductors," in Superionic Conductors, ed. by G. D. Mahan and W. L. Roth, Plenum Press (New York, 1976).

17. J. Lefèvre, Ann. Chim., 8, 135 (1963).

18. R. Collongues, F. Queyroux, M. Perez y Jorba and J. C. Gilles, Bull. Soc. Chim. Fr., 1141 (1965).

19. M. R. Thornber, D. J. M. Bevan and J. Graham, Acta Cryst., B24, 1183 (1968).

20. J. G. Allpress and H. J. Russell, J. Solid State Chem., 15, 68 (1975).

21. R. E. Carter and W. L. Roth, "Conductivity and Structure in Calcia-stabilized Zirconia," in Electromotive Force Measurements in High-Temperature Systems, ed. by C. B. Alcock, Elsevier (New York, 1968).

22. D. Michel, Mater. Res. Bull., 8, 943 (1973).

23. D. Michel, Rev. Int. Hautes Tempar. Refract., 9, 225 (1972).

24. B. Hudson and P. T. Moseley, J. Solid State Chem., 19, 383 (1976).

25. W. H. Rhodes and R. E. Carter, J. Am. Ceram. Soc., 49, 244 (1966).

26. A. S. Nowick, Columbia University, private communication.

27. J. Griffith, Columbia University, private communication.

28. J. E. Bauerle, J. Phys. Chem. Solids, 30, 2657 (1969).

29. K. S. Cole and R. H. Cole, J. Chem. Phys., 9, 341 (1941).

U.S. DEPT. OF COMM. BIBLIOGRAPHIC DATA SHEET	1. PUBLICATION OR REPORT NO. NBSIR 77-1270	2. Gov't Accession No.	3. Recipient's Accession No.

4. TITLE AND SUBTITLE

Materials for Fuel Cells

5. Publication Date

6. Performing Organization Code

7. AUTHOR(S) L. H. Bennett, M. I. Cohen, A. L. Dragoo, A. D. Franklin, A. J. McAlister and K. F. Young

8. Performing Organ. Report No. 3130456

9. PERFORMING ORGANIZATION NAME AND ADDRESS

NATIONAL BUREAU OF STANDARDS
DEPARTMENT OF COMMERCE
WASHINGTON, D.C. 20234

10. Project/Task/Work Unit No.

11. Contract/Grant No.

12. Sponsoring Organization Name and Complete Address *(Street, City, State, ZIP)*

Division of Conservation Research and Technology
U.S. Energy Research and Development Administration
Washington, D. C. 20545

13. Type of Report & Period Covered

Annual Report

14. Sponsoring Agency Code

15. SUPPLEMENTARY NOTES

16. ABSTRACT *(A 200-word or less factual summary of most significant information. If document includes a significant bibliography or literature survey, mention it here.)*

This report describes the first year's progress of the NBS program on Materials for Fuel Cells.

Transition metal carbides, borides and nitrides ("refractory hard metals') were examined with respect to stability and to catalytic oxidation of H_2 as non-precious substitutes for Pt as fuel electrocatalysts. Hydrogen oxidation was observed only on Pt, WC and $(Mo_{0.8}W_{0.2})C$. The activity of WC was found to depend upon the preparative method. The compound $(Mo_{0.8}W_{0.2})C$, which has the WC structure, was estimated to have a specific activity from 1.5 to 3 times greater than that of the WC samples.

A versatile automated system for electrochemical analysis was designed and built utilizing the precision of digital control and readout techniques to perform essentially analog measurements. The automated system uses a microprocessor as the key element in the central processing unit. The various components and operation of the automated system are described.

Studies of CeO_2:Y_2O_3 ceramic electrolytes were designed to measure the influence of annealing and prolonged current passage on electrical properties of these materials. Work on a high temperature facility for these experiments and preparation of CeO_2:Y_2O_3 ceramic specimens is described.

AC impedance was measured on several CeO_2:Y_2O_3 sintered specimens as a function of frequency using a network analyzer. The features of this instrument and the theory of the measurements are presented.

17. KEY WORDS *(six to twelve entries; alphabetical order; capitalize only the first letter of the first key word unless a proper name; separated by semicolons)*

AC impedance; automated electrochemical analysis; ceramic electrolytes; ceria-yttria; cyclic voltammetry; electrocatalysis; equivalent circuit; fuel cells; microprocessor; network analyzer; phosphoric acid electrolyte; refractory hard metals.

18. AVAILABILITY

[X] Unlimited

[ ] For Official Distribution. Do Not Release to NTIS

[ ] Order From Sup. of Doc., U.S. Government Printing Office Washington, D.C. 20402, SD Cat. No. C13

[X] Order From National Technical Information Service (NTIS) Springfield, Virginia 22151

19. SECURITY CLASS (THIS REPORT)	21. NO. OF PAGES
UNCLASSIFIED	69
20. SECURITY CLASS (THIS PAGE)	22. Price
UNCLASSIFIED	$4.50